JLAB-THY-00-21
UND-HEP-00-BIG 05

Precision Studies of Duality in the 't Hooft Model

Richard F. Lebed [a*] and Nikolai G. Uraltsev [b,c†]

[a] *Jefferson Lab, 12000 Jefferson Avenue, Newport News, VA 23606, U.S.A.*
[b] *Dept. of Physics, Univ. of Notre Dame du Lac, Notre Dame, IN 46556, U.S.A.*
[c] *Petersburg Nuclear Physics Institute, Gatchina, St. Petersburg, 188350, Russia*

(June, 2000)

Abstract

We address numerical aspects of local quark-hadron duality using the example of the exactly solvable 't Hooft model, two-dimensional QCD with $N_c \to \infty$. The primary focus of these studies is total semileptonic decay widths relevant for extracting $|V_{cb}|$ and $|V_{ub}|$. We compare the exact channel-by-channel sum of exclusive modes to the corresponding rates obtained in the standard $1/m_Q$ expansion arising from the Operator Product Expansion. An impressive agreement sets in unexpectedly early, immediately after the threshold for the first hadronic excitation in the final state. Yet even at higher energy release it is possible to discern the seeds of duality-violating oscillations. We find the "Small Velocity" sum rules to be exceptionally well saturated already by the first excited state. We also obtain a convincing degree of duality in the differential distributions and in an analogue of $R_{e^+e^-}(s)$. Finally, we discuss possible lessons for semileptonic decays of actual heavy quarks in QCD.

PACS numbers: 12.38.Aw, 11.10.Kk, 13.20.-v

*lebed@jlab.org
†uraltsev@undhep.hep.nd.edu

Contents

1 Introduction

Questions of how to compare hadronic observables to the apparent underlying fundamental theory of QCD lie at the heart of understanding the nature of strong interactions. Thirty years after its inception, QCD in $D=4$ spacetime dimensions still stubbornly refuses to admit a global solution. The asymptotic freedom property of the theory permits the perturbative calculation of (Euclidean) Green functions involving large values of momentum transfer or energy release in terms of quarks and gluons, the fundamental objects of QCD. But at lower scales one enters the nonperturbative regime, which not only invalidates (or at least complicates) the standard perturbative methods of field theory developed in QED, but also leads to a dramatic change in the physical spectrum of the theory. Instead of quarks and gluons, only colorless hadrons are produced as asymptotic states in any process, even at arbitrarily large energy.

Many nontrivial theoretical techniques respecting QCD first principles have been developed to study nonperturbative features of the theory. Yet despite numerous advances, no one has been able to compute the masses, wavefunctions, or transition amplitudes of hadrons in terms of quark masses and couplings directly from the QCD Lagrangian. Moreover, many existing theoretical tools are expressed through various expansions in certain small parameters; the actual range of each parameter where the expansions are applicable is often not well known. In such a situation, it is clearly

advantageous to build a soluble toy field theory that incorporates as many features of the QCD Lagrangian as possible.

Such a theory does indeed exist, the famous 't Hooft model [1], which is defined by the Yang-Mills Lagrangian in $D=2$ spacetime dimensions in the limit of a large number of colors N_c. As was shown in the original paper, the quark-antiquark sector of the theory admits an infinite tower of confined, color-singlet solutions that can be obtained, in principle, to an arbitrary degree of numerical accuracy. The reason for this solubility lies precisely in the defining features of the model. Large N_c eliminates all Feynman diagrams with internal $q\bar{q}$ loops and nonplanar gluons. On the other hand, $D=2$ allows gluon self-couplings to be eliminated by gauging away one component of the gauge potential A^μ. Since only two components are initially present, the commutator term $[A^\mu, A^\nu]$ in the covariant derivative, which gives gluon self-coupling, vanishes identically in such gauges. Then the only remaining Feynman diagrams to be summed for the quark-antiquark Green function are "rainbow" and "ladder" diagrams, whose Schwinger-Dyson equations can be solved, giving rise to an integral expression called the 't Hooft equation (discussed in Sec. 2).

The 't Hooft model provides an excellent laboratory for testing various approaches to strong interaction physics. After all, the 't Hooft equation provides a means to compute hadronic masses, wavefunctions, and transition amplitudes in terms of the underlying partonic degrees of freedom.

In this work we are specifically interested in questions of local quark-hadron duality in the inclusive decays of heavy quarks. The notion of duality in general terms was first introduced in the early days of QCD in Ref. [2] but not pursued for quite some time. A more detailed consideration was given a few years ago by Shifman [3] and later reiterated in a number of papers (see, e.g., Refs. [4, 5]), with applications relevant to Minkowskian observables amenable to study via an operator product expansion (OPE). This allows the formulation of the concept of local duality in a more quantitative way, including nontrivial nonperturbative effects; we refer the reader to these recent publications for the theoretical aspects. Here the question of duality is studied concretely by comparing the weak decay width of a meson containing a heavy quark computed in two ways. In terms of partonic degrees of freedom, one has an OPE depending upon the free quark diagram (with perturbative corrections) and a number of nonperturbative matrix elements suppressed by powers of the heavy quark mass. In terms of the hadronic degrees of freedom, one simply computes the weak decay amplitude for each allowed exclusive channel, and adds them up one by one. This comparison is especially instructive since one may consider the behavior of solution as the mass m_Q of the heavy decaying quark is varied.

Such a problem was first considered in Ref. [6], where the main elements in numerical computations of exclusive decay rates were annunciated. The hadronic result was compared to the Born-level free-partonic diagram as a function of m_Q. In terms of the OPE, the latter is the tree-level piece of the Wilson coefficient corresponding to the unit operator. The numerical agreement was seen to be remarkable, in that the onset of the asymptotic agreement was clearly visible already for relatively small val-

ues of m_Q. The intrinsically limited numerical accuracy for sufficiently heavy quarks, however, prohibited drawing a definite conclusion about the size of nonperturbative corrections for asymptotically large m_Q. Additional numerical studies [7] considered similar questions for weak decay topologies other than the simple spectator tree diagram, in particular weak annihilation (WA).

The validity of the OPE was addressed analytically in Refs. [5, 8, 9], which considered on one hand the nature of the OPE for heavy quark decays, and on the other an explicit $1/m_Q$ expansion of the decay amplitudes, which allows an analytical summation of the individual decay rates in the asymptotic regime. The agreement of the two approaches through relative order $1/m_Q^4$ was obtained by means of a number of sum rules derived directly from the 't Hooft equation, the archetype of which first appeared in Ref. [10].

While adequate to illustrate the theoretical validity of the OPE for the inclusive decay widths of heavy flavors, the analytic methods per se cannot help in answering the practical question relevant to phenomenology of beauty and charm quarks: Namely, how accurately do the OPE-improved parton computations describe the true weak decay width of a heavy flavor meson with finite mass, only a few times larger than the typical strong interaction scale? A purely analytic expansion can hardly be used for this purpose, since it is a priori unknown how small an expansion parameter must be for the expansion to start yielding a reasonable approximation, not to mention achieving the necessary precision. To obtain insights into the size of deviations between the actual decay widths and the expressions obtained from the OPE for quarks in the intermediate mass range, one must employ real numerical computations.

In this paper we focus on semileptonic decays of heavy quarks. In the contexts of both real QCD and the 't Hooft model, they are technically simpler than nonleptonic decays. Moreover, the magnitude of local duality violation is phenomenologically most important in semileptonic decays when one extracts $|V_{cb}|$ and $|V_{ub}|$. We use the techniques developed in Ref. [6] to evaluate the required decay rates, and confront the total decay width with the expansion in terms of a power series in $1/m_Q$ of Ref. [5]. Moreover, by making use of a number of relations derived in the large-m_Q limit of the 't Hooft equation [11], members of the set of nonperturbative matrix elements involved can be related to each other, providing an economical description of the nonperturbative physics. These are the tools that allow us to study the onset of quark-hadron duality.

As explained in Appendix A, we use a scheme based on the modified Multhopp method, by which the 't Hooft equation is converted into an infinite-dimension eigenvector system that for practical reasons must be truncated at some number N of eigenvector modes. The asymptotic convergence of this approach has not been rigorously studied, although it apparently must yield unlimited accuracy when the number of the Multhopp modes N goes to infinity. Yet the rate of convergence at large N is not well known. Additionally, large quark masses turn out to require one to use a larger N for sufficient numerical accuracy, as discussed in Sec. 2. It therefore seems

mandatory to make an independent cross-check of the numerical accuracy. We investigate this problem by comparing the numerical values of a number of static properties of heavy mesons at different values of m_Q, with the results of their $1/m_Q$ expansions obtained analytically from the 't Hooft equation; this is the topic of Sec. 3. We find that our solutions have sufficient numerical accuracy for masses m_Q corresponding to physical values (in the sense explained in Sec. 3) as large as 20 GeV.

The duality of the inclusive widths of heavy-flavor hadrons to the parton-level widths, including the power corrections from the OPE, emerges through a set of sum rules that equate sums of weighted transition probabilities to possible final states and expectation values of the local heavy quark operators. Since our main interest lies in $b \to c$ transitions, which carry in practice a limited energy release, the most relevant are the so-called small velocity (SV) sum rules, which we study here in the heavy quark limit. The behavior of these sum rules not only shapes the semileptonic $b \to c$ decays in actual QCD, but is also important for the determination of the basic parameters of the heavy quark expansion.

An additional advantage of the heavy quark limit for our investigation is that we are able to compute the SV amplitudes semi-analytically, using the exact relations [11] derived from the 't Hooft equations and relying for input only on a few static parameters, which can be computed with a high precision. A discussion of these relations appears in Sec. 4. We find that the SV sum rules in the 't Hooft model are saturated to an unexpectedly high degree by the first excitation above the ground state (which we henceforth call the "P-wave" excitation, despite the fact that in $D=2$ only radial excitations occur). Its contributions to even the Darwin (ρ_D^3) and kinetic (μ_π^2) expectation values constitute over 90% and 96% of the totals, respectively, while it saturates the "optical" sum rule for $M_B - m_b$ to a 1.5% accuracy. This appears to be an intriguing dynamical feature of the model. A similar high-saturation effect has been observed in a quark flux-tube model [12], for the contribution from the "valence" quarkonium states.

We study the size of violations of local duality in the semileptonic decays $b \to c\,\ell\bar{\nu}$ assuming vectorlike weak currents and massless leptons. These assumptions are important for comparison with QCD far beyond the obvious parallel of closely resembling the actual world: The strength of the resonance-related duality violation crucially depends on the threshold behavior in the decay probabilities, which is completely different in two and four dimensions. The two-body phase space, while $\propto |\vec{p}|$ in $D=4$, is $\propto 1/|\vec{p}|$, that is, infinite at threshold, in $D=2$. On the other hand, the situation is special for massless leptons: Their invariant mass is always zero if they are produced by a vectorlike source, and the weak vertex is then proportional to the momentum. As a result, in this case the threshold behavior of the decay rate becomes $\propto |\vec{p}|$ much in the same way as in real QCD. This is a crucial detail if one tries to draw practical lessons from the 't Hooft model. The need for a vectorlike coupling in $D=2$ is even more stark for the parton-level calculation. There one finds that the integrated three-body phase space actually diverges for massless leptons, and only the behavior of the weak decay amplitude renders the width finite. We provide more

arguments in favor of such a choice in Sec. 5, which is dedicated to the inclusive decay widths.

In Sec. 6 we briefly illustrate how well the duality works for the vacuum correlator of light quarks in the timelike domain. In the context of the heavy quark expansion this is relevant for the nonleptonic decay widths, including spectator-dependent effects like WA.

Section 7 summarizes our investigation and discusses the conclusions that can be drawn for actual QCD.

Appendices describe the computational technique employed and contain a number of relations for the heavy quark limit of the 't Hooft equation employed in these numerical studies.

2 The 't Hooft Equation and Its Solutions

We first review some well-known properties of the 't Hooft model both as a reminder and to establish notation. Confinement is manifest in 1+1 spacetime dimensions with large N_c, and the quark(m_1)-antiquark($\overline{m}_2$) two-particle irreducible Green function, i.e., the meson wavefunction $\varphi(x)$, is given by the 't Hooft equation:

$$M_n^2\,\varphi_n(x) = \left(\frac{m_1^2-\beta^2}{x} + \frac{m_2^2-\beta^2}{1-x}\right)\varphi_n(x) - \beta^2 \int_0^1 \mathrm{d}y\,\varphi_n(y)\,\mathrm{P}\frac{1}{(y-x)^2}\;, \qquad (1)$$

where x is the momentum fraction in light-cone coordinates carried by the quark, and

$$\beta^2 \equiv \frac{g_s^2}{2\pi}(N_c - 1/N_c)\;. \qquad (2)$$

Since β is finite in the large-N_c limit, it provides a natural unit of mass. Thus, all masses in this paper are understood as multiples of β. Indeed, as pointed out in Ref. [6], β fills the role in 1+1 dimensions of served by $\Lambda_{\rm QCD}$ in 3+1. We discuss the estimation of β as a particular number in Sec. 3.

The singularity of the QCD Coulomb interaction in Eq. (1) is regularized using a principal value prescription, indicated by P in Eq. (1).

Solutions $n = 0, 1, \ldots$ of the 't Hooft equation alternate in parity, with the lowest being a pseudoscalar. The general analytic solution in closed form is not known. As the eigenvalue index n increases, the eigenvalues M_n^2 asymptotically approach $\beta^2[\pi^2 n + O(\ln n)]$.

The static limit $m_1 \equiv m_Q \to \infty$ is most easily studied [8, 10, 11] by employing the "nonrelativistic" variables $M_n = m_Q + \epsilon_n$, $t = (1-x)m_Q$ and $\Psi_n(t) = \frac{1}{\sqrt{m_Q}}\varphi_n\Big(1-\frac{t}{m_Q}\Big)$, in terms of which Eq. (1) assumes the form

$$\epsilon_n \Psi_n(t) \;=\; \frac{m_2^2-\beta^2}{2t}\Psi_n(t) + \frac{t}{2}\Psi_n(t) - \frac{\beta^2}{2}\int_0^\infty \mathrm{d}s\,\frac{\Psi_n(s)}{(t-s)^2}\;. \qquad (3)$$

We solve the finite-mass 't Hooft equation using a numerical method called the Multhopp technique [13], a venerable system for solving integral equations with singular kernels. It was first applied to the 't Hooft equation in Ref. [14]. The idea is to expand the wavefunction in a series of modes, not unlike Fourier analysis, and then turn the equations for the mode coefficients into an equivalent infinite-dimension eigenvector problem. In practice, one then truncates at some point where the higher modes are deemed to have little effect upon the wavefunction solutions, which is of course strongly dependent on the highest value of n used. The detailed formulas for applying the *standard* Multhopp technique to mesons with unequal quark masses in the 't Hooft model appear in Appendix A of Ref. [6].

Intrinsic to the original Multhopp technique is the evaluation of the wavefunction at a discrete set of points called "Multhopp angles," which in the current problem are equivalent to

$$x_k = \frac{1}{2}\left[1 + \cos\left(\frac{k\pi}{N+1}\right)\right] , \qquad k = 1, \ldots, N , \tag{4}$$

where N is the number of modes retained in the numerical solution. The mode coefficients are then obtained by the use of a discrete inversion formula [(A7) in [6]]. However, the Multhopp solutions can be seen to vanish as $\sqrt{x}$ and $\sqrt{1-x}$ at the endpoints $x = 0$ and $x = 1$, respectively [see (A10)–(A11) in [6]], while the exact solutions are known to vanish as x^{γ_1} and $(1-x)^{\gamma_2}$, respectively, where

$$\frac{m_i^2}{\beta^2} \, + \, \pi\gamma_i \cot \pi\gamma_i \; = \; 1 \, , \tag{5}$$

leading to a type of Gibbs phenomenon in the Multhopp solutions. Since the Multhopp angles cease to sample the wavefunction at some finite distance from the endpoints, it may be expected that the wavefunctions thus obtained are numerically inaccurate there. This shortcoming led Brower, Spence, and Weis [15] to improve the Multhopp technique by eliminating the Multhopp angles and using instead a continuous inversion formula. The algebraic details are presented in Appendix A, and it is this improved numerical technique that is used in obtaining our results.

3 Heavy Quark Expansion and Cross Check of the Algorithm

Let us first establish a bit of notation. The mass of a heavy quark of flavor Q is labeled as $m_1 \to m_Q$; in the weak transitions considered in subsequent sections, the final-state quark q is assigned the mass m_q. The spectator antiquark mass m_2 is labeled by m, or $m_{\rm sp}$ if there is any chance of confusion.

As explained in the previous section and Appendix A, we use the modified Multhopp technique to find numerical solutions of the 't Hooft eigenstate problem. Since

the heavy meson wavefunctions are peaked near the end of the interval, the accuracy deteriorates with increasing m_Q. The same, in principle, applies to the high excitations of light hadrons. A more appropriate strategy for heavy quarks is to start with a solution of the infinite-mass (static) equation. This has been done analytically [5, 8], and full consistency[3] with the OPE was demonstrated.

However, our practical interest lies in the properties of heavy hadrons with m_Q lying in the intermediate domain, specifically for m_Q one order of magnitude larger than β. The convergence of the $1/m_Q$ expansion in this case is too difficult to quantify analytically. This is just the situation where the numerical computations are best employed.

Therefore, an important element of the analysis is to check the accuracy of the numerical computations of both the heavy hadron masses and wavefunctions at different values of m_Q. To this end, we compute the masses and certain moments for the ground and first excited states, and compare them to the analytic $1/m_Q$ expansion. In general, the terms in the $1/m_Q$ expansion depend on a number of expectation values in the static limit, like the kinetic one $\mu_\pi^2 = \left\langle \bar{Q}(i\vec{D}\,)^2 Q \right\rangle$, etc. However, one can show [11] that the parameters appearing here through high order in $1/m_Q$ can be expressed in terms of just the asymptotic value $\overline{\Lambda} = M_{H_Q} - m_Q$ and the corresponding decay constant. These quantities are the ones most accessible to numerical evaluation; in particular, $\overline{\Lambda}$ is expected to be the most accurately determined quantity.

Our main computations refer to the case of $m_{\rm sp} = 0.56\beta$, as chosen in Ref. [6]. It corresponds (see Sec. 4) to a mass of the strange quark in QCD. The choice of a noticeable light quark mass may be motivated by an attempt to mimic the effect of the transverse gluons absent in $D = 2$, which in a certain respect supply some effective mass to the light quark. Clearly, this can be only a rather crude approximation, since the bare quark mass breaks chiral invariance. One can suppose, nevertheless, that this side effect is not too important for our purposes. The chiral symmetry is spontaneously broken anyway, and the presence of a massless versus a massive pion does not seem to be essential for the range of problems we address here. On the other hand, the effect of the transverse degrees of freedom is known to soften the $x \to 1$ singularity of the heavy quark distribution function [10, 16, 17], similar to the impact of the light quark mass in the 't Hooft model. The behavior of the distribution function affects the inclusive decays of the heavy quarks in an essential way.

We also present some results for $m_{\rm sp} = 0.26\beta$, partly to explore light quark dependences of matrix elements and partly to investigate the beginnings of failure of the numerical solutions as $m_{\rm sp} \to 0$. The number N of Multhopp modes used is 500; we considered smaller N as well to study this dependence, but since the behavior was found to be stable, we do not dwell on it further here.

[3] In the case that the fermions f created by the weak current have $m_f = 0$, this agreement was shown up to and including $O(1/m_Q^4)$ terms in the weak decay width in [5], while terms up to and including $O(m_f^2/m_Q)$ were shown to coincide with those in the OPE in [8]. In the current work we take $m_f = 0$.

The masses of heavy hadrons obey [5, 8, 18]

$$M_{H_Q} - m_Q \;=\; \overline{\Lambda} + \frac{\mu_\pi^2 - \beta^2}{2m_Q} + \frac{\rho_D^3 - \rho_{\pi\pi}^3}{4m_Q^2} \;+\; O\!\left(\frac{\beta^4}{m_Q^3}\right) . \tag{6}$$

where

$$\begin{aligned} \mu_\pi^2 &= \left\langle \bar{Q}(i\vec{D}\,)^2 Q \right\rangle , \;\; \rho_D^3 \;=\; -\frac{1}{2}\left\langle \bar{Q}(\vec{D}\cdot\vec{E})Q \right\rangle , \\ \rho_{\pi\pi}^3 &= -\frac{1}{2}\left\langle iT\{\bar{Q}(i\vec{D}\,)^2 Q(x), \bar{Q}(i\vec{D}\,)^2 Q(0)\}\right\rangle_{q=0} , \end{aligned} \tag{7}$$

and these expectation values refer to the infinite mass limit. In the $\rho_{\pi\pi}^3$ expression, q is the momentum variable conjugate to x, and diagonal transitions within the correlator have been removed.

Since $\overline{\Lambda}$ in QCD traditionally denotes the mass difference between a ground-state pseudoscalar meson and its corresponding heavy quark in the large m_Q limit [as it is defined in Eq. (6)], and we need it for a number of the excited states $H_Q^{(n)}$ as well, we assign the notation

$$\overline{\Lambda}^{(n)} \equiv \epsilon^{(n)}, \tag{8}$$

and use ϵ and $\overline{\Lambda}$ throughout the paper on equal footing. Equations (6)–(14) hold for each state $H_Q^{(n)}$ with $n = 0, 1, \ldots$, so that an implicit superscript (n) is to be understood in these expressions.

According to Ref. [11], the following relations hold in the 't Hooft model:

$$\mu_\pi^2 = \frac{\overline{\Lambda}^2 - m^2 + \beta^2}{3} , \qquad \rho_D^3 = \frac{\beta^2 F^2}{4} , \qquad \rho_{\pi\pi}^3 = \frac{1}{36}\left[8\overline{\Lambda}(\overline{\Lambda}^2 - m^2 + \beta^2) + 3\beta^2 F^2\right] . \tag{9}$$

Here F is the scaled decay constant in the heavy quark limit, i.e.,

$$F^{(n)} \;=\; \int_0^\infty \mathrm{d}t\, \Psi_n(t) \;=\; \lim_{m_Q\to\infty} \int_0^{m_Q} \mathrm{d}t\, \frac{1}{\sqrt{m_Q}}\, \phi_n\!\left(1 - \frac{t}{m_Q}\right) \;=\; \lim_{m_Q\to\infty} c_n \sqrt{m_Q} , \tag{10}$$

where the superscript is suppressed if there is no ambiguity,

$$c_n = \int_0^1 \mathrm{d}x\, \varphi_n(x) , \tag{11}$$

and the exact relation between c_n and the decay constant of the nth excitation is given in Eq. (68). In the heavy quark limit one has

$$\overline{\Lambda} = m_Q \langle 1 - x \rangle \;, \qquad \mu_\pi^2 = m_Q^2 \left(\left\langle x^2 \right\rangle - \langle x \rangle^2 \right) \;, \tag{12}$$

but there are $O(1/m_Q)$ corrections to these relations. For further applications to the decay widths we also consider the scalar expectation value [5]

$$\frac{1}{2M_{H_Q}} \left\langle \bar{Q}Q \right\rangle \;=\; \frac{m_Q}{M_{H_Q}} \left\langle \frac{1}{x} \right\rangle . \tag{13}$$

Then the following expansions hold:

$$\begin{aligned}
\sqrt{m_Q}\, c_n &= \left(1 - \frac{2[2\epsilon^{(n)} - m(-1)^n]}{3m_Q}\right) F^{(n)} + O\left(\frac{\beta^{5/2}}{m_Q^2}\right), \\
m_Q \langle 1-x \rangle &= \overline{\Lambda} - \frac{\overline{\Lambda}^2 + \mu_\pi^2}{m_Q} + \frac{4\overline{\Lambda}(6\overline{\Lambda}^2 + 8\mu_\pi^2 + 3\beta^2) + \beta^2 F^2}{24 m_Q^2} + O\left(\frac{\beta^4}{m_Q^3}\right), \\
m_Q^2 \left(\left\langle x^2 \right\rangle - \langle x \rangle^2\right) &= \mu_\pi^2 - \frac{1}{3m_Q}\left(8\overline{\Lambda}\mu_\pi^2 + \beta^2 F^2\right) + O\left(\frac{\beta^4}{m_Q^2}\right), \\
\frac{m_Q}{M_{H_Q}} \left\langle \frac{1}{x} \right\rangle &= 1 - \frac{\mu_\pi^2 - \beta^2}{2m_Q^2} - \frac{\rho_D^3 - \rho_{\pi\pi}^3}{2m_Q^3} + O\left(\frac{\beta^4}{m_Q^4}\right). \qquad (14)
\end{aligned}$$

We note that values of μ_π^2, ρ_D^3, or $\rho_{\pi\pi}^3$ determined from the expansions Eqs. (14) suffer degraded numerical accuracy compared to those taken directly from Eqs. (9) since $\overline{\Lambda}$ and F are determined from more stable expansions (in particular, they do not depend upon close numerical cancellations). Therefore, we use Eqs. (9) as primary information and relegate Eqs. (14) to numerical checks. Our method of determining $\overline{\Lambda}$ from the $M_{H_Q} - m_Q$ expression, designed to minimize the influence of potentially large uncertainties at large m_Q, is described in Appendix C.

Values of $M_{H_Q} - m_Q$ and and the averages in Eqs. (14) as functions of m_Q from $m = 0.56\beta$ to 50β are presented in Table 1 for both the ground and first excited states. Similar results for just the ground state with $m = 0.26\beta$ are presented in Table 2. Based upon the 10 data points presented in Table 1 for the ground state, one may fit to a polynomial in $1/m_Q$, obtaining

$$\begin{aligned}
\frac{1}{\beta}(M_{H_Q} - m_Q) &= 1.317 - 0.086\frac{\beta}{m_Q} - 0.050\frac{\beta^2}{m_Q^2} + O\left(\frac{\beta^3}{m_Q^3}\right), \\
c_0 \sqrt{\frac{m_Q}{\beta}} &= 2.032 - 2.775\frac{\beta}{m_Q} + O\left(\frac{\beta^2}{m_Q^2}\right), \\
\frac{m_Q}{\beta} \langle 1-x \rangle &= 1.316 - 2.491\frac{\beta}{m_Q} + 3.789\frac{\beta^2}{m_Q^2} + O\left(\frac{\beta^3}{m_Q^3}\right), \\
\frac{m_Q^2}{\beta^2} \left(\left\langle x^2 \right\rangle - \langle x \rangle^2\right) &= 0.8074 - 4.050\frac{\beta}{m_Q} + O\left(\frac{\beta^2}{m_Q^2}\right), \\
\frac{m_Q}{M_{H_Q}} \left\langle \frac{1}{x} \right\rangle &= 1 + 0.099\frac{\beta^2}{m_Q^2} - 0.044\frac{\beta^3}{m_Q^3} + O\left(\frac{\beta^4}{m_Q^4}\right). \qquad (15)
\end{aligned}$$

The corresponding expressions using the approach of Appendix C (neglecting the one for $M_{H_Q} - m_Q$, which is used as input and hence is identical through $O(\beta^2/m_Q^2)$) read

$$\begin{aligned}
c_0 \sqrt{\frac{m_Q}{\beta}} &= 2.035 - 2.816\frac{\beta}{m_Q} + O\left(\frac{\beta^2}{m_Q^2}\right), \\
\frac{m_Q}{\beta} \langle 1-x \rangle &= 1.318 - 2.544\frac{\beta}{m_Q} + 4.512\frac{\beta^2}{m_Q^2} + O\left(\frac{\beta^3}{m_Q^3}\right),
\end{aligned}$$

$$\frac{m_Q^2}{\beta^2}\left(\left\langle x^2\right\rangle - \langle x\rangle^2\right) = 0.8078 - 3.996\frac{\beta}{m_Q} + O\left(\frac{\beta^2}{m_Q^2}\right),$$
$$\frac{m_Q}{M_{H_Q}}\left\langle\frac{1}{x}\right\rangle = 1 + 0.096\frac{\beta^2}{m_Q^2} - 0.066\frac{\beta^3}{m_Q^3} + O\left(\frac{\beta^4}{m_Q^4}\right). \qquad (16)$$

This agreement between the two approaches is quite excellent and is exhibited in Figs. 1–4 for $M_{H_Q} - m_Q$ and the quantities in Eqs. (14); in general, the exact results are presented as points on a solid line, while each fit using Eqs. (16) is presented as a dashed line. In Fig. 6 the analogous expression $M_{H_Q} - m_Q$ for the $m = 0.56\beta$ first excited state is presented, while Fig. 7 uses the same methods and values from Table 2 to present $M_{H_Q} - m_Q$ for the $m = 0.26\beta$ ground state. In Fig. 1 and especially in Fig. 7, the quality of numerical results is seen (as expected) to begin breaking down at large m_Q and small m, since $N = 500$ is fixed. We conclude that the numerical routine we rely upon is sufficiently accurate for $N = 500$ up to $m_Q \approx (25 \div 30)\beta$. The critical value of m_Q also depends, however, on the meson's light quark mass, decreasing for small m. This is expected since at small m the sharpness of the wavefunction as $x \to 1$ becomes stronger, and more Multhopp functions are required to approximate it: Each Multhopp function vanishes like $\sqrt{1-x}$. Likewise, the required N increases for the excited states. Still, one can check that it is possible to go as high as $m_Q = 15\beta$ even for m as small as 0.1β.

It turns out that a numerically significant cancellation occurs in the value of $\mu_\pi^2 - \beta^2$ in $1/m_Q^2$ corrections and, in particular, at the $1/m_Q^3$ level between ρ_D^3 and $\rho_{\pi\pi}^3$, for the ground state just around our primary value $m = 0.56\beta$. Such a numerical suppression of the power corrections is accidental and does not occur for the excited states, nor for $m = 0.26\beta$.

Let us note that the expectation value of the *light-quark* scalar density in the heavy meson turns out very close to unity for the ground state, which may be seen by taking $m_Q \leftrightarrow m$ and $x \leftrightarrow 1-x$ in Eq. (13) and referring to Table 3; this is a characteristic feature of a nonrelativistic (with respect to the light quark) bound-state system. It implies an almost simple additive dependence of $\overline{\Lambda}$ on the light quark mass m,

$$\overline{\Lambda} \simeq \overline{\Lambda}_{|m=0} + m\,, \qquad (17)$$

and indeed one can verify this feature by comparing $M_{H_Q} - m_Q$ values between Table 1 ($m = 0.56\beta$) and Table 2 ($m = 0.26\beta$). While this pattern is expected when the spectator quark is heavy, it a priori needs not hold when it is light. This supports the naive expectation that the chiral symmetry breaking may lead to a description in some aspects resembling the nonrelativistic constituent quark model. The above expectation value, however, decreases for the excited states, as expected from such a picture.

Drawing semi-quantitative conclusions for QCD requires a translation rule between the mass parameters in the two theories, that is, an estimate of the value of β in GeV. Different dimensionful quantities can be taken as the yardstick; since the theories are not identical, this translation rule must be introduced with some care.

As follows from the heavy quark sum rules, the physics of duality in the decay widths of heavy flavors crucially depends on the properties of the lowest excited heavy-quark states, in particular the P-wave excitations with opposite parity to the ground-state multiplet. It will become evident from the next section that they are of primary importance for the $1/m_Q$ expansion of static properties as well. Therefore, we choose the mass difference between the lowest parity-even (P-wave) state and the parity-odd ground-state meson to gauge the translation between the mass scales.

In the 't Hooft model the mass difference $\epsilon_1 - \epsilon_0$ for light spectators amounts to about 1.3β. Real charm spectroscopy suggests that the first P-wave excitations are between 400 and 500 MeV above the ground state. Taking the larger value for sake of illustration, we arrive at the estimate

$$\beta \;\approx\; 400\,\mathrm{MeV}\;, \tag{18}$$

which is adopted in our analysis. This falls rather close to the estimate of Ref. [19], which relied on a quite different type of effects in the light-quark systems.

Assuming a value for the "bare" b quark mass in QCD (normalized at the appropriate scale $\gtrsim m_b$) of about 4 GeV, we conclude that mesons with quarks of masses

$$m_b \approx 10\beta\;,\quad m_c \approx (2.5 \div 3.5)\beta\;, \tag{19}$$

represent in the 't Hooft model the actual beauty and charm mesons.

The value of $\overline{\Lambda} \simeq 1.3\beta \approx 500\,\mathrm{MeV}$ seems to be in a reasonable correspondence with the size of this difference in QCD when it is normalized at a low hadronic scale, $\overline{\Lambda}(1\,\mathrm{GeV}) \approx (600 \pm 60)\,\mathrm{MeV}$ [20].

It should be noted, however, that the kinetic expectation value in the 't Hooft model turns out to be rather small, $\mu_\pi^2 \simeq 0.8\beta^2 \approx 0.12\,\mathrm{GeV}^2$. This is not surprising, since the chromomagnetic field is absent in two dimensions, while it was shown [18, 21, 22] to be crucial in the real case. Indeed, the comparison is better justified for the difference $\mu_\pi^2 - \mu_G^2$ in actual QCD versus the value of μ_π^2 in the 't Hooft model. These questions were discussed in detail in Ref. [23], and can be easily understood using the sum rule representation. Due to the absence of spin in two dimensions, there is no difference between the would-be spin-1/2 and spin-3/2 light degrees of freedom. In particular, labeling the "oscillator strengths" τ defined in the next section by spin rather than excitation number, $\tau_{1/2} = \tau_{3/2}$ and $\epsilon_{1/2} = \epsilon_{3/2}$ effectively hold. Then the sum

$$\mu_\pi^2 \;=\; 3\sum_n \epsilon_n^2 |\tau_{1/2}|^2 \;+\; 6\sum_n \epsilon_n^2 |\tau_{3/2}|^2 \;\to\; 9\sum_n \epsilon_n^2 |\tau_{1/2}|^2\;, \tag{20}$$

and the latter sum is just the general expression for $\mu_\pi^2 - \mu_G^2$:

$$\mu_\pi^2 - \mu_G^2 \;=\; 9\sum_n \epsilon_n^2 |\tau_{1/2}|^2\;. \tag{21}$$

Accepting such an identification suggested in Ref. [23] and the estimate $\mu_\pi^2 - \mu_G^2 \simeq (0.15 \pm 0.1)\,\mathrm{GeV}^2$, we again observe a reasonable agreement with the findings of the 't Hooft model.

4 Duality in the SV Sum Rules

A useful theoretical limit—the so-called small velocity (SV) regime—was suggested in the mid 80's [24] as a theoretical tool for studying semileptonic heavy quark decays. This refers to kinematics where both b and c quarks are heavy, but the energy release is limited, so that the velocity of the final charm hadron is small. At large energy release the OPE for the width must converge rapidly to the actual hadronic width. Still, at fixed energy release the deviations, although $1/m_Q$ suppressed, are present regardless of the absolute values of masses.

In the SV regime the semileptonic decays proceed either to the ground-state charm final state, D or D^* (the semi-elastic transitions), or to excited "P-wave" states of the opposite parity. Other decays are suppressed by higher powers of velocity, or by heavy quark masses.

The equality of the sum of partial decay widths and its OPE expansion is achieved through the sum rules that relate the sums of the P-wave transition probabilities, weighted with powers of the excitation energies, to the static characteristics of the decaying heavy hadron. The onset of convergence of the OPE expansion for the widths is then directly related to the pattern of saturation of the sum rules by the lowest excitations. If higher states contribute significantly, they delay the onset of duality, while their absence leads to a tight quark-hadron duality after the first P-wave channel is open.

Knowledge of degree of saturation of the heavy quark sum rules is also important for another reason: It determines the hadronic scale above which one can apply the perturbative treatment to compute corrections or account for evolution of the effective operators. The lower this scale, the more predictive in turn is the treatment of the nonperturbative effects in the OPE.

A recent review of the SV sum rules can be found in Ref. [22] (the perturbative aspects are discussed in more detail in Ref. [23]). For most practical purposes addressed here, one can consider the perturbative effects to be absent in the 't Hooft model. In particular, the heavy quark parameters do not depend perturbatively on the normalization point, and there is no need in the explicit ultraviolet cutoff to introduce a normalization point. The sum rules we address are

$$\rho_k^2 - \frac{1}{4} = \sum_n \tau_{nk}^2 \,, \tag{22}$$

$$\frac{1}{2}\,\overline{\Lambda}_k = \sum_n (\epsilon_n - \epsilon_k)\,\tau_{nk}^2 \,, \tag{23}$$

$$\left(\mu_\pi^2\right)_k = \sum_n (\epsilon_n - \epsilon_k)^2\,\tau_{nk}^2 \,, \tag{24}$$

$$\left(\rho_D^3\right)_k = \sum_n (\epsilon_n - \epsilon_k)^3\,\tau_{nk}^2 \,. \tag{25}$$

Here k and n denote excitation indices for the initial and final states, respectively (in practice only transitions from the ground state are interesting, so we limit ourselves

to $k=0$; in this case the index k is omitted). The so-called "oscillator strengths" τ parameterize the transition amplitudes into the opposite-parity states in the SV limit,

$$\frac{1}{2m_Q}\left\langle n\left|\bar{Q}\gamma_\mu Q\right|k\right\rangle \;=\; \tau_{nk}\,\epsilon_{\mu\nu}v^\nu \;+\; O(\vec{v}^3), \tag{26}$$

where $\vec{v}$ is the velocity of the final state hadron. In the diagonal transition ρ_k^2 is the slope of the Isgur-Wise (IW) function of state $|k\rangle$:

$$\frac{1}{2m_Q}\left\langle k(\vec{v})\left|\bar{Q}\gamma_0 Q\right|k(0)\right\rangle \;=\; 1-\rho_k^2\frac{\vec{v}^2}{2} \;+\; O(\vec{v}^4)\;. \tag{27}$$

The expressions for τ_{nk} and ρ_k in terms of the light-cone wavefunctions are

$$\begin{aligned}
\tau_{nk} &= \int_0^\infty \mathrm{d}t\,\Psi_n(t)\,t\frac{\mathrm{d}}{\mathrm{d}t}\Psi_k(t) = -\lim_{m_Q\to\infty}\int_0^1 \mathrm{d}x\,\varphi_n(x)\,(1-x)\frac{\mathrm{d}}{\mathrm{d}x}\varphi_k(x),\\
\rho_k^2 &= \int_0^\infty \mathrm{d}t\,\left|\left(t\frac{\mathrm{d}}{\mathrm{d}t}+\frac{1}{2}\right)\Psi_k(t)\right|^2 = \lim_{m_Q\to\infty}\int_0^1 \mathrm{d}x\,\left|\left[(1-x)\frac{\mathrm{d}}{\mathrm{d}x}-\frac{1}{2}\right]\varphi_k(x)\right|^2\;.
\end{aligned} \tag{28}$$

The finite-m_Q corrections to the x-integral forms turn out to be rather significant, leading to significant problems in precision numerical studies. To avoid this problem we use the analytic expression for the inelastic amplitudes obtained in Ref. [11]:

$$\tau_{nk}=\left\langle n\left|t\frac{\mathrm{d}}{\mathrm{d}t}\right|k\right\rangle \;=\; -\frac{\beta^2}{2(\epsilon_n-\epsilon_k)^3}\,F^{(n)}F^{(k)}\left(\frac{1-(-1)^{n-k}}{2}\right)\;, \tag{29}$$

where $F^{(n)}$ are the asymptotic values of the decay constants c_n scaled up by the factor $\sqrt{m_Q}$, as in Eq. (10). The constants $F^{(n)}$ are computed as the values of $c_n\sqrt{m_Q}$ at $m_Q=15\beta$ (see Table 1) augmented by the $1/m_Q$ corrections detailed in the first of Eqs. (14), while values of ϵ_n are computed using the procedure described in Appendix C.

The results of the computations for the case $m_Q=15\beta$, $m=0.56\beta$ are presented in Table 4. Our central result is a surprisingly good saturation of the sum rules: The first ($n=1$) excitation generates 99.4% of ρ^2, 98.5% of $\overline{\Lambda}$, 96% of μ_π^2, and even 91% of ρ_D^3. The rest is almost completely saturated by the second P-wave state ($n=3$), where the cumulative values for the same quantities read 99.92%, 99.73%, 99.1%, and 96.7%, respectively.

In terms of absolute numbers, the sum rules Eqs. (22)–(25) would give $\rho^2-1/4=0.529$, $\overline{\Lambda}=1.278\beta$, $\mu_\pi^2=0.782\beta^2$, and $\rho_D^3=0.99\beta^3$, the last of which gives $F^{(0)}=1.99\sqrt{\beta}$, in fine agreement with the values obtained from the values obtained in the previous section via the methods described in Appendix C. The few-percent discrepancy corresponds to the accuracy in determinations of squared decay constants.

The level of saturation by the lowest open channels is extraordinary. The explicit reason for such a perfect saturation of the sum rules involving even rather high,

$\sim \epsilon^3$ powers of the excitation energy can be read off Eq. (29)—τ's are inversely proportional to the third power of the excitation energy. With the asymptotics $\epsilon_n \sim \sqrt{n}$, $F^{(n)} \sim n^{-1/4}$, the first excitation energy $\epsilon_1 - \epsilon_0$ is notably smaller than the next one $\epsilon_3 - \epsilon_0$ including three energy gaps. The general peculiarity of the 't Hooft model leading to such a saturation is not understood completely.

With this pattern of saturation of the SV sum rules for the ground-state meson, one expects an early onset of the accurate duality for the inclusive widths in the $b \to c$ transitions, only slightly above the threshold of the first excitation. Demonstrating this result through direct evaluation of the decay widths is one of the purposes of the next section.

5 Local Duality in the Decay Widths

The semileptonic widths described in this work were considered in detail in Ref. [5]. Here we recapitulate a few basic points. The weak decay Lagrangian is

$$\mathcal{L}_{\rm weak} \;=\; -\frac{G}{\sqrt{2}}\,(\bar{c}\gamma_\mu b)\,(\bar{e}\gamma^\mu \nu)\;. \tag{30}$$

In terms of the previous notation, $Q \to b$, $q \to c$ (or, later in this section, u), and $H_Q \to B$. The key property of all $D=2$ vectorlike currents is that for $m_e = m_\nu = 0$, the invariant mass q^2 of the lepton pair is always zero. For all computational purposes decays into this massless lepton pair are equivalent to decays into a single massless pseudoscalar particle ϕ weakly coupled to quarks according to

$$\tilde{\mathcal{L}}_{\rm weak} \;=\; -\frac{G}{\sqrt{2\pi}}\,\bar{c}\gamma_\mu b\,\epsilon^{\mu\nu}\,\partial_\nu \phi\;. \tag{31}$$

Several arguments favor our choice of a vectorlike weak decay interaction in the 't Hooft model. One is of course the simplicity of Eq. (31). Another is that for $q^2 = 0$ some difficult problems of renormalization are absent, as we now discuss. The central problem in applying the OPE in practice is disentangling perturbative and nonperturbative effects. More precisely, this refers to the separation of short-distance effects attributed to the coefficient functions from long-distance effects residing in the matrix elements of the effective heavy-quark operators.

The perturbative corrections, for example those that renormalize the weak quark current, are generally rather nontrivial, even in the 't Hooft model. However, according to the nonrenormalization theorem of Ref. [5], such vertex corrections are absent from the decays with $q^2 = 0$. This allows one to isolate the problem of renormalization of the underlying current from the question of interest in our study: possible deviations of the full decay widths due to the presence of thresholds in the production of the hadronic resonances.

In reality, from the OPE viewpoint some short-distance corrections still remain even in this special kinematic region due to the high-momentum tails in the meson wavefunctions. These tails come from the hard gluon exchanges between the

constituents. In principle, these "hard" components can also be separated from the "soft" bound-state dynamics explicitly. However, in practice this is not necessary: These effects are completely contained in the meson wavefunctions.

Another advantage of vectorlike currents is apparent when one notes that the $D=2$ three-body "semileptonic" phase space diverges logarithmically for massless leptons. Explicitly, for the decay $M \to m+m_\ell+m_\ell$ (equal lepton masses are assumed to render the expressions simpler), the three-body phase space turns out to be

$$\begin{aligned}\Phi_3(M;m,m_\ell,m_\ell) &= \frac{1}{4\pi^3(M-m)\sqrt{(M+m)^2-4m_\ell^2}} \\ &\quad \times K\left[\frac{(M+m)^2\,[(M-m)^2-4m_\ell^2]}{(M-m)^2\,[(M+m)^2-4m_\ell^2]}\right], \end{aligned} \tag{32}$$

where K is the complete elliptic integral of the first kind. As $m_\ell \to m$, one regains Eqs. (4.1)–(4.3) of [6], while as $m_\ell \to 0$, the argument of the elliptic integral goes to unity, and $K(1-\epsilon) \to \ln(8/\epsilon)/2$. This is a manifestation of the logarithmic infrared divergence of the massless scalar Green function at large distance in $D=2$. A detailed calculation shows that the vector nature of the weak coupling regularizes the phase space integral, preventing the partonic rate from diverging in the limit of massless leptons. Furthermore, as discussed in the Introduction, this also removes the $1/|\vec{p}|$ singularity in the threshold behavior for hadronic two-body decays.

As a final advantage of vectorlike currents and the special kinematic point $q^2=0$, note that at $q^2=0$ the $B \to D^{(n)}$ transition amplitudes are directly expressed in terms of the overlap between the initial and the final wavefunctions:

$$q_\mu \frac{1}{2M_B}\langle n|\epsilon^{\mu\nu}J_\nu|B\rangle = -q_z \int_0^1 \mathrm{d}x\, \varphi_n(x)\varphi_B(x)\,, \tag{33}$$

where $q_z = -|\vec{p}| = -(M_B^2 - M_n^2)/2M_B$, so that the partial decay width for $B \to D^{(n)}\,\ell\bar{\nu}$ is given by

$$\Gamma_n = \frac{G^2}{4\pi}\cdot\frac{M_B^2-M_n^2}{M_B}\left|\int_0^1 \mathrm{d}x\,\varphi_n(x)\varphi_B(x)\right|^2 \theta(M_B-M_n)\,. \tag{34}$$

The threshold suppression mentioned above is manifested in the explicit factor $(M_B^2-M_n^2)$: The reciprocal of this factor in the phase space is removed by q_z^2 from the matrix element. It is also possible to derive this result directly using the methods of Ref. [6]; note, however, that these expressions are much simpler than those of Ref. [6], because the vectorlike current with massless leptons restricts q^2 to 0. The sum of these widths over all open channels is to be compared to the OPE prediction. The remarkable speed of saturation in n, anticipated in the last section, is illustrated for one sample case in Table 5.

Turning to the OPE, we mention one more problem associated with an accurate understanding of local duality violation. Apart from the purely theoretical aspect

that OPE power series are generally only asymptotic and, thus have a formally zero radius of convergence in $1/m_Q$, one normally has additional practical limitations. Only a limited number of the terms, as well as the associated expectation values, are usually known, which places additional theoretical uncertainties that dominate in practice at sufficiently large m_Q.

This feature can be naturally incorporated in the analysis of our concrete model. We account completely only through terms that scale like $1/m_Q^4$, the highest order that emerges from the OPE free from the four-fermion operators [5]. The rest, although calculable in principle term-by-term in the 't Hooft model, are taken to represent the OPE "tails" discarded by the unavoidable truncation.

Using the sum rules of the 't Hooft model, Ref. [5] established the following exact representation for the total decay width:

$$\Gamma_B = \frac{G^2}{4\pi}\cdot\frac{m_b^2-m_c^2}{M_B}\int_0^1\frac{\mathrm{d}x}{x}\,\varphi_B^2(x)\;-\sum_{M_n>M_B}\Gamma_n, \tag{35}$$

where Γ_n at $M_n > M_B$ are understood as given by Eq. (34) without the explicit θ-function singling out the open channels; such Γ_n are therefore all negative. On the other hand, the OPE yields the result

$$\Gamma_B = \frac{G^2}{4\pi}\cdot\frac{m_b^2-m_c^2}{m_b}\left[\frac{m_b}{M_B}\int_0^1\frac{\mathrm{d}x}{x}\,\varphi_B^2(x)\,+\,O\left(\frac{\beta^5}{M^5}\right)\right]\,, \tag{36}$$

with M generically denoting the OPE expansion parameter; we do not specify here if it is m_b or $m_b - m_c$, or some other combination. It was shown in Ref. [5] that the Γ_n term in Eq. (35) is dual to the order term in Eq. (36); however we do not use this here and rather treat the latter as an intrinsic uncertainty in the "practical" version of the OPE.

Thus, our strategy is to compare the exact width

$$\Gamma_B = \frac{G^2}{4\pi}\sum_{M_n<M_B}\frac{M_B^2-M_n^2}{M_B}\left|\int_0^1\mathrm{d}x\varphi_n(x)\varphi_B(x)\right|^2, \tag{37}$$

to

$$\Gamma_{\rm OPE} = \frac{G^2}{4\pi}\cdot\frac{m_b^2-m_c^2}{m_b}\cdot\frac{m_b}{M_B}\int_0^1\frac{\mathrm{d}x}{x}\,\varphi_B^2(x)\,. \tag{38}$$

The expectation value $\frac{m_b}{M_B}\left\langle\frac{1}{x}\right\rangle$ above can either be evaluated numerically, or in the spirit of the OPE, computed in the form of a $1/m_b$ expansion, the last of Eqs. (14). It turns out that the expansion converges very rapidly to the exact result, so that this does not significantly affect the observed pattern of local duality at the quantitative level. The Born-term partonic rate is simply given by $\Gamma_{\rm OPE}$ with this expectation value set to unity,

$$\Gamma_b = \frac{G^2}{4\pi}\cdot\frac{m_b^2-m_c^2}{m_b}. \tag{39}$$

The main practical interest of these calculations lies in the $b \to c$ width with its limited energy release E_r. In general, E_r can be small either if m_b is not large enough, or even at large m_b if $E_r = m_b - m_c$ (or $m_b - m_c - \sqrt{q^2}$ if q^2 is nonzero) is insufficient due to a significant c quark mass. The latter case falls into the SV category, and the violations of duality are suppressed here even at the maximal q^2 by heavy quark symmetry, as was pointed out in the mid-80's [24]. Therefore, one a priori expects a different pattern in the two cases. We try to separate the possible effects by considering different choices for m_b and m_c rather than by only taking them close to their realistic values.

With these arguments in mind, one can expect to find significant effects of duality violation in the cases where $1/m_c$ or $1/m_b$ effects are important. As suggested in Ref. [23], in this case it is advantageous to fix m_b close to its actual value, and vary m_c from near m_b down to smaller values, changing in this way the energy release. At one end of the interval the local duality is supported by the heavy quark symmetry with large quark masses and SV kinematics, while at another end it rests on the large energy release.

We start from the SV case when m_b is fixed and large and m_c is large as well, varying the energy release by increasing m_c towards m_b. Since the violation of local duality is expected to be suppressed for all values of m_c, high numerical accuracy is vital. We fix $m_b = 15\beta$ ($\approx 6\,\mathrm{GeV}$), and vary m_c from 5β up to m_b. The results are given in Table 6 and Fig. 8. We note that the difference between the two widths is so small that one must plot $\ln(\Gamma_B/\Gamma_{\mathrm{OPE}} - 1)$ rather than the widths themselves. This is expected since the SV sum rules are very well saturated, as detailed in the previous section—the higher thresholds are then strongly suppressed numerically at finite energy release. But for m_c approaching m_b, where they could be noticeable, the heavy quark symmetry works efficiently since both quarks are very heavy. In fact, the only prominent features on the plot occur when thresholds to the first few D states of opposite parity to the ground-state B meson are crossed, for example between $m_c = 13.5$ and 14β. The deviation is extremely small also for smaller m_c where the c quark velocity is rather large—yet there the energy release is significant, and a large number of excited states (up to 18 at $m_c = 5\beta \approx 2\,\mathrm{GeV}$) are produced. Table 7 and Fig. 9 show analogous results for $m_b = 10\beta$, $m = 0.56\beta$.

To render the duality violation more apparent, we consider (Table 8 and Fig. 10) the same decay widths for a b quark with half the mass, $m_b = 5\beta \approx 2\,\mathrm{GeV}$. Even here the deviation is below per mill as soon as the first excitation can appear with sufficient phase space. The duality-violating component at last exhibits the proper oscillating behavior (note the decrease between $m_c = 3$ and 3.5β or 1 and 1.5β), but this effect is too small to be extracted reliably at larger energy release where this property becomes an asymptotic rule.

As follows from our computations, local duality is violated at a tiny level in the $b \to c$ decays in the 't Hooft model whenever it is a priori meaningful to apply OPE. A possible reason behind this might be that for unidentified reasons the heavy quark symmetry works for the inclusive widths too effectively, down to relatively low masses

and velocities of order 1. This was conjectured in the early papers on the subject [24].

Therefore, our final attempt in the quest for the sizeable duality violation in beauty is considering the $(b\to u)$-type transitions, where the heavy quark symmetry per se does not constrain the individual transition form factors. We fix in our expressions $m_c = m = 0.56\beta$ or 0.26β (but still keep the two quarks flavor-distinguished) and vary m_b from $1\beta \approx 0.4\,\mathrm{GeV}$ to $12\beta \approx 4.5\,\mathrm{GeV}$. The results are shown in Table 9 and Fig. 11, and Table 10 and Fig. 12, respectively. Although the difference between the actual width and its OPE approximation is larger, it still is very small and approaches a percent level for m_b as low as $2\beta \approx 0.8\,\mathrm{GeV}$. The total decay width is no longer saturated to such a high degree by transitions to the ground state, especially for larger m_b. Nevertheless, the duality is amazingly well satisfied when just the first few open channels are summed. Again, the only prominent features in the plots appear when crossing kinematic thresholds due to the lightest D mesons of opposite parity to the ground-state B.

The extraordinary agreement between Γ_B and Γ_{OPE} may be underscored by instead plotting (Fig. 13, final column of Table 9) the difference between Γ_B and the Born-term partonic rate Γ_b given in Eq. (39). From an algebraic point of view, Γ_B and Γ_{OPE} differ generically at $O(1/M^5)$, while Γ_B and Γ_b begin to differ already at $O(1/M^2)$.

Thus, we find local duality between the actual semileptonic decay width and its OPE expansion to be very well satisfied in all cases.

Before concluding this section, let us briefly address duality in the differential distribution $\Gamma^{-1}\,\mathrm{d}\Gamma/\mathrm{d}E$. In the heavy quark limit the shape of the final-state hadronic mass distribution follows the heavy quark distribution function in the decaying meson; for the $b\to u$ decays under consideration, this is the light-cone distribution function $F(x)$. In decays with $q^2 = 0$ the recoil energy of the lepton pair E is directly related to the final state mass M_h:

$$E = \frac{M_B^2 - M_h^2}{2M_B}\,. \tag{40}$$

Since $q^2 = 0$, these decays are analogous to $b \to s\gamma$ in the Standard Model. In the large-m_b limit one has

$$\frac{1}{\Gamma}\,\frac{\mathrm{d}\Gamma}{\mathrm{d}E} \;=\; \frac{2}{\overline{\Lambda}}\,F\left(\frac{2E - m_b}{\overline{\Lambda}}\right)\,. \tag{41}$$

At finite m_b in a theory with narrow resonances the actual distribution is given by the comb of δ-functions with spacing in the argument of Eq. (41) of order $\overline{\Lambda}/m_b$. In order to obtain a continuous result, we adopt the simple ansatz of averaging over the peaks. Using Eq. (40) to define the energy E_n of the nth state M_h, we integrate the δ-function for the nth state evenly over the energy range $(E_n + E_{n+1})/2$ to $(E_n + E_{n-1})/2$, i.e., the midpoints between energy eigenvalues. Letting N be the maximum number of kinematically allowed M_h values, we establish the endpoint bins by defining $E_{-1} = E_{\max} = M_B/2$ and $E_{N+1} = E_{\min} = 0$.

We find that our numerical computations yield a distribution resembling the light-cone distribution function φ^2; specifically,

$$F(y) \;=\; \overline{\Lambda}\Psi^2\left((1-y)\overline{\Lambda}\right) \;=\; \lim_{m_Q\to\infty}\frac{\overline{\Lambda}}{m_Q}\varphi^2\left(1-(1-y)\frac{\overline{\Lambda}}{m_Q}\right)\;. \tag{42}$$

Recalling that $M_B = m_b + \overline{\Lambda} + O(1/m_b)$ and combining Eqs. (41) and (42) yields

$$\frac{1}{\Gamma}\frac{\mathrm{d}\Gamma}{\mathrm{d}E} \approx \lim_{m_Q\to\infty}\frac{2}{m_Q}\varphi^2\left(1-\frac{M_B-2E}{m_Q}\right). \tag{43}$$

The two sides of this expression are plotted in Fig. 14, using $m_Q = 25\beta$ to represent the limit $m_Q \to \infty$, while the actual distribution is considered at $m_b = 10\beta$. The agreement is quite remarkable. The continuous distribution appears to pass approximately through the midpoint of each bin; owing to the near-equal spacing of 't Hooft model eigenvalues in M_n^2, Eq. (40) shows that these bin midpoints are very close to the values E_n themselves.

It is also interesting to consider integration over a range of E. In particular, define $\Phi(1-2E/M_B)$ as the cumulative fractional width from maximum energy $M_B/2$ down to the given E; then $\Phi(0) = 0$ and $\Phi(1) = 1$. While the exact result for $\sum \Delta\Gamma/\Gamma$ amounts to an integration of the δ-function differential widths renormalized so that the cumulative result approaches unity, the integral of the continuous distribution gives

$$\Phi(y) = \lim_{m_Q\to\infty}\;\frac{2}{m_Q}\int_0^y \mathrm{d}z\,\varphi^2\left(1-\frac{M_{H_Q}}{m_Q}z\right). \tag{44}$$

These two curves are presented in Fig. 15. Two features particularly stand out in this plot. First, even for m_b as large as $10\beta \approx 4\,\mathrm{GeV}$, the overwhelming part of the decay probability falls into the transitions to at most four lowest states. Second, the continuous curve seems to provide a nearly optimal description possible for the step-like exact distribution. The point-to-point deviation for all plotted values with $1-2E/M_B > 0.04$ does not exceed half of the contribution of the nearest threshold.

6 Duality in the Vacuum Current Correlator

In this section we briefly illustrate the onset of duality for the absorptive part of the vector current correlator with light quarks, of the type that determines the normalized cross section $R(e^+e^- \to \text{hadrons})$ as a function of energy. In the context of the heavy quark decays this is relevant in nonleptonic decay widths in two kinds of processes: in spectator-independent decays, where $R(q^2)$ determines the weight with which the semileptonic width at given q^2 must be integrated over q^2 (see Ref. [8]), and in the effects of WA decays.

In either case, at $N_c \to \infty$ the cross section appears as a comb-like collection of δ-functions:

$$R(q^2) \;=\; \sum_n c_n^2\,\delta(q^2-M_n^2)\;; \qquad c_n = \int_0^1 \mathrm{d}x\,\varphi_n(x)\;. \tag{45}$$

The above expression for the residues refers to the case where a vector current is considered. We suppress here the factor of $\sqrt{N_c/\pi}$ relating c_n to f_n [Eq. (68)]. We also assume in what follows that the light quark masses are equal, $m_u = m_d$, and are $O(\beta)$ or less, in order to reach asymptotic q^2 more quickly.

In the extreme situation of infinitely narrow resonances one cannot, of course, discuss a point-to-point equality of the cross section $R(q^2)$ with its OPE in the form of $1/q^2$ expansion. A meaningful comparison is possible if each resonant peak is somehow averaged over an interval no smaller than the distance between adjacent peaks, the latter being approximately given by $\Delta q^2 \simeq \pi^2\beta^2$ [1]. It is worth recalling that $R(q^2)$ is proportional to m^2/q^4, so one must consider nonvanishing masses for the vector current, and address the OPE terms formally suppressed by m^2/q^2.

This question was first addressed in the context of nonleptonic decays in Ref. [7] using the numerical approach. Duality for the average cross section in the same manner as above, i.e., using sum rules derived from the 't Hooft equation and analytically matching terms in the $1/m_Q$ expansion, was obtained in Ref. [8]. Yet establishing the asymptotics per se cannot tell us beforehand how early one can expect the onset of duality. Here we study this question numerically, in the domain of intermediate q^2.

The concrete amount of the deviation between $R(q^2)$ and $R^{\rm OPE}(q^2)$ in the case of direct resonances may depend in an essential way on the chosen smearing procedure. Interested in the qualitative features only, we choose a rather simplified, crude method: We spread the integral of $R(q^2)$ evenly over the interval between the successive resonances. More precisely, we put

$$\bar{R}(q^2) \;=\; \frac{1}{M^2_{2n+1}-M^2_{2n-1}}\int_{M^2_{2n-1}}^{M^2_{2n+1}} {\rm d}q^2 R(q^2) \;=\; \frac{c^2_{2n}}{M^2_{2n+1}-M^2_{2n-1}}\,, \qquad (46)$$

for $M^2_{2n-1} < q^2 < M^2_{2n+1}$, with $M^2_{-1} = 4m^2$, the partonic pair production threshold. Here we use the fact that c_n vanish for odd n when $m_u = m_d \equiv m$. This smearing is very similar to that described for the differential width in the last section, except that averaging is performed in q^2 rather than E. The free quark loop $R(q^2)$, which is of course the leading term of the OPE, is given by

$$R_0(q^2) \;=\; \frac{2m^2}{q^4}\frac{1}{\sqrt{1-4m^2/q^2}}\,. \qquad (47)$$

Table 11 and Fig. 16 show the results for our reference case $m = 0.56\beta$. The agreement of the average hadronic cross section with the parton-computed probability again turns out to be very good. Apparently, this can be related to two facts: the heavy suppression of power corrections to $R(q^2)$ in the OPE (see Eqs. (34)–(35) in [8]), and an early onset of the asymptotics in the spectrum,

$$M^2_{n+1} - M^2_n \;\simeq\; \pi^2\beta^2\,, \qquad (48)$$

which even at $n = 0$ is satisfied to about 15%.

7 Discussion and Summary

The main motivation behind the present study has been to assess the magnitude of local duality violations in the inclusive semileptonic decays of beauty particles. We considered this question using the 't Hooft model as a toy theory in which all relevant decay amplitudes can be evaluated numerically. The 't Hooft model, while retaining certain key features of full $D = 4$ QCD that shape the spectrum of hadrons (quark confinement, chiral symmetry breaking), still differs from $D = 4$ in many respects. Yet using it as a lab for exploration carries an important advantage—it allows no "wiggle room" for interpretation of the results. There are no ad hoc parameters to choose or adjust, and as soon as the underlying weak decay Lagrangian is fixed, the numerical results are unambiguous and must be accepted at face value. This positively distinguishes this approach from various models where often the conclusions, even qualitatively, depend on the arbitrary choice of parameters according to one's preferences. The question of a particular model being compatible with the general dynamical properties of QCD underlying the OPE approach, often quite problematic in simplified quark models, does not arise for the 't Hooft model.

Although the simplest illustration of the asymptotic nature of the decay width $1/m_Q$ expansion and related violations of local duality [3] follows just from the existence of hadronic thresholds (see, e.g., [8]), violation of local duality is a more universal phenomenon that is *not* directly related to existence of hadronic resonances nor even confinement itself. This has been illustrated in Ref. [4] by the example of soft instanton effects that do not lead, at least at small density, to quark confinement—but do indeed generate computable oscillating duality-violating contributions to the total decay rates.

Nevertheless, there is a widespread opinion that decays with manifest resonance structure in the final state are most difficult for—if compatible at all with—the standard OPE. Even the possibility that the OPE does not fully apply in the case of "hard" confinement has been occasionally voiced in the literature. The analytic studies performed in Refs. [5, 8, 9], which explicitly demonstrate in the 't Hooft model the applicability of the OPE to the total widths, should help to allay such conceptual concerns. Nevertheless, the intuition remains that resonance dominance is not "favorable" for the OPE, and problems might show up, for instance, through a delayed numerical onset of duality, in that the approximate equality of the OPE predictions and the actual decay widths may set in only after a significant number of thresholds has been passed. To address such issues, the 't-Hooft model seems to represent the most certain testing ground for local duality in the domain of decays of moderately heavy quarks.

Contrary to naive expectations, we found surprisingly accurate duality between the (truncated) OPE series for $\Gamma_{\rm sl}$ and the actual decay widths. The deviations are suppressed to a very high degree almost immediately after the threshold for the first excited final state hadron is passed. No suspected delay in the onset of duality was found.

The key property that governs the onset of the $1/m_Q$ expansion for the semileptonic widths is the pattern of saturation of the heavy quark sum rules. We examined a particular class, the SV sum rules in the heavy quark limit, that has the most transparent quantum mechanical meaning. We found them saturated to an amazing degree by the very first excitation. The contribution of the remaining, higher states to the slope of the IW function, $\overline{\Lambda}$, and μ_π^2 does not exceed a few percent. Even in the Darwin operator sum rule, the first excitation accounts for 90% of the whole expectation value, despite the fast-growing weight, $(\epsilon_k - \epsilon_0)^3$ of higher-order contributions. This peculiarity underlies the early onset of duality for the case when initial- and final-state quarks are both heavy.

Some of the duality-violating features observed in these studies have natural explanations. At fixed energy release $m_Q - m_q$ the magnitude of the deviations is smaller if m_Q, m_q are both large (as in $b \to c$) than if they are both small. This is expected, since in the former case the heavy quark symmetry for the elastic amplitude additionally enforces approximate duality even when no expansion in large energy release can be applied.

It is interesting, however, that at fixed m_b the duality violation decreases rapidly as m_c decreases, in full accord with the OPE where the higher order terms are generally suppressed by powers of $1/(m_b - m_c)$. This is clearly a *dynamical* feature that goes beyond heavy quark symmetry per se, the quality of which deteriorates as m_c decreases.

It is also instructive to note that including the calculated power-suppressed OPE terms significantly reduces the difference between the actual decay width and its purely partonic evaluation. Moreover, the seeds of oscillations inherent to duality violation (as functions of quark masses), can be seen. Since we adopted the truncated OPE expansion to mirror the existing implementation of the OPE in QCD, the deviations do not average to zero but rather oscillate around the (rapidly dissipating) contributions attributed to discarded higher-order terms.

The numerical effects of duality violation we study turn out to be typically quite small. Partially this can be attributed to moderate size of the corresponding expectation values multiplying $1/m_Q^k$ corrections in the OPE. Yet certainly not all power corrections in heavy quarks are suppressed in the model. It is well known from ordinary quantum mechanics that masses (eigenvalues) typically are much more robust against perturbations than wavefunctions themselves (or transition amplitudes). We observe a similar pattern in the 't Hooft model. For example, $1/m_Q$ corrections to the meson decay constants turn out very significant even at the scale of the b quark mass. Apparently, the inclusive decay rates fall into the class of "robust" observables, although, as explained above, this was difficult to anticipate beforehand.

We note here another "fragile" observable, the light-cone heavy quark distribution function, which can be measured in decays of the type $b \to s\gamma$. In $D = 2$ the scaled spread $m_Q^2 \left(\langle x^2 \rangle - \langle x \rangle^2 \right)$ of the x distribution approaches μ_π^2 at large m_Q. Yet, as seen in Fig. 4, even at the b quark mass one would obtain from this distribution only about 60% of the actual value of μ_π^2, due to significant $1/m_Q$ corrections. This caveat may

be important for existing analyses of the decay distributions in B decays, where such effects routinely are not included.

We also briefly addressed the inclusive differential decay distributions in the analogues of $b \to u\,\ell\bar{\nu}$ or $b \to s\gamma$ decays. Generally, we find good agreement (at the scale corresponding to the physical b mass) with the parton-based prediction incorporating effects of the "Fermi motion," and in particular for the partially integrated probability

$$\Phi(x) \,=\, \frac{1}{\Gamma_{\rm sl}} \int_0^{xM_B^2} {\rm d}M_h^2\, \frac{{\rm d}\Gamma_{\rm sl}}{{\rm d}M_h^2}\,. \tag{49}$$

This distribution, following Refs. [25, 26], is examined in real B decays in the quest for $|V_{ub}|$ [27]. However, the point-to-point deviations are clearly still significant, for the decays to only the 4 or 5 lowest final states saturate the overwhelming fraction of the total decay probability. It is quite conceivable, though, that such deviations are less pronounced in actual QCD owing to the significant resonance widths and to a richer resonance structure.

The vacuum current correlator also turns out to be especially robust; even neglecting all OPE corrections except the leading partonic contribution leads to excellent agreement with the hadronic result.

Turning to the direct phenomenological conclusions that can be inferred from our studies, we see that, to the extent our findings can be transferred to real QCD, violation of local duality in the total semileptonic widths of B mesons is not an issue. The scale of duality violation lies far below the phenomenologically accessible limits, and cannot affect the credibility of $|V_{cb}|$ or $|V_{ub}|$ extractions.

In reality there are, of course, essential conceptual differences between the two theories, including those aspects that are expected to be essential for local duality (for a discussion, see Ref. [8]). Although many seem to optimistically suggest that duality violation is more pronounced in the 't Hooft model than for actual heavy flavor hadrons, some differences may still work in the opposite direction. In $D=2$ there are no dynamical gluons, nor a chromomagnetic field that in $D=4$ provides a significant scale of nonperturbative effects in heavy flavor hadrons. Likewise, there is no spin in $D=2$, and no corresponding P-wave excitations of the light degrees of freedom (the so-called $j=3/2$ states), which seem to play an important role in $D=4$.

Two-dimensional QCD neither has long perturbative "tails" of actual strong interactions suppressed weakly (by only powers of logs of the energy scale). In $D=2$ the perturbative corrections are generally power-suppressed, as follows from the dimension of the gauge coupling. As discussed in Ref. [8], it is conceivable that the characteristic mass scale for freezing out the transverse gluonic degrees of freedom is higher than in the "valence" quark channels. This would imply a possibly higher scale for onset of duality in α_s/π corrections to various observables.

Regardless of these differences, we conclude that presence of resonance structure per se is not an obstacle for fine local quark-hadron duality tested in the context of the OPE. As we see in the 't Hooft model, resonances themselves do not seem to demand a larger duality interval. As soon as the mass scale of the states saturating

the sum rules in a particular channel (quark or hybrid) has been passed, the decay width can be well approximated numerically by the expansion stemming from the OPE.

The ground states of heavy mesons in the 't Hooft model exhibit relatively small expectation values of nonperturbative operators (μ_π^2, ρ_D^3, but not $\overline{\Lambda}$) compared to real QCD, if our identification $\beta \simeq 400\,\mathrm{MeV}$ is adopted. This may be regarded as a reason for small duality violation for Γ_{sl} in the model. However, even if we scale β up to 700–800 MeV to make up for smallness of the nonperturbative OPE effects, the duality violation is still very small, and superficially rather insignificant even in charm.

We note, however, that the specific choice Eq. (30) of the weak interaction effectively requires decays to occur only at $q^2=0$, and therefore the effects of four-fermion operators of the type $(\bar{Q}\Gamma q)(\bar{q}\Gamma Q)$ are totally absent, at least in the lowest orders of perturbation theory (cf. Ref. [5], Sec. III.B.3). As was suggested in Ref. [28], it is conceivable that the apparent excess in $\Gamma_{\mathrm{sl}}(D)$ is simply related to a noticeable magnitude of the non-valence (nonfactorizable) expectation values $\langle D\,|(\bar{c}\Gamma s)\,(\bar{s}\Gamma c)|\,D\rangle$. If this conjecture is true, similar effects in $\Gamma_{\mathrm{sl}}(B\to X_u\ell\nu)$ are still suppressed but possibly detectable in future precision experiments. In the context of the present study, it suffices to say that this would be a legitimate OPE effect rather than a manifestation of a significant local duality violation in the strict sense.

Acknowledgments: R.L. thanks the Department of Energy for support under Contract No. DE-AC05-84ER40150; N.U. acknowledges the support of the NSF under grant number PHY96-05080, by NATO under the reference PST.CLG 974745, and by RFFI under grant No. 99-02-18355. We are grateful to N. Isgur for inspiring interest and discussions, and to M. Burkardt for invaluable insights. N.U. also thanks I. Bigi, M. Shifman and A. Vainshtein for encouraging interest and collaboration on related issues, and A. Zhitnitsky for useful comments. N.U. enjoyed the hospitality of Physics Department of the Technion and the support of the Lady Davis grant during completion of this paper.

A The BSW Improvement of the Multhopp Technique

The Brower-Spence-Weis [15] (BSW) improvement of the Multhopp technique avoids the need for evaluating the wavefunction at a discrete set of points called "Multhopp angles," thus improving the behavior of the solutions in the endpoint regions, as described in Sec. 2. Here we exhibit the expressions used by BSW, correcting along the way some minor typographical errors in their work.

Starting with the 't Hooft equation (1) with bare quark masses m_1 and m_2, one

converts the kinematic variables x, y to angular variables:

$$x = \frac{1+\cos\theta}{2}, \qquad y = \frac{1+\cos\theta'}{2}\ , \tag{50}$$

in terms of which the 't Hooft equation reads

$$\begin{aligned} \frac{M_p^2}{2}\,\varphi_p(\theta) &= \left[\frac{m_1^2}{1+\cos\theta} + \frac{m_2^2}{1-\cos\theta}\right]\varphi_p(\theta) \\ &\quad + \int_0^\pi \mathrm{d}\theta'\,\varphi_p(\theta')\,\mathrm{P}\frac{1}{(\cos\theta-\cos\theta')^2}. \end{aligned} \tag{51}$$

Expanding

$$\varphi_p(\theta) \;=\; \sum_{n=1}^{\infty} a_n^{(p)} \sin n\theta, \tag{52}$$

and using the continuous inversion identity (contrast with Eq. (A7) of Ref. [6])

$$\int_0^\pi \mathrm{d}\theta\ \sin m\theta\ \sin n\theta \;=\; \frac{\pi}{2}\,(\delta_{mn}-\delta_{m,-n})\,, \tag{53}$$

one obtains the infinite-dimensional eigenvector system

$$M_p^2 a_n^{(p)} \;=\; (H_0+V)_{nm}\,a_m^{(p)}\ , \tag{54}$$

where

$$(H_0)_{nm} \;=\; +\frac{4}{\pi}\int_0^\pi \mathrm{d}\theta\,\left[\frac{m_1^2}{1+\cos\theta}+\frac{m_2^2}{1-\cos\theta}\right]\sin n\theta\,\sin m\theta, \tag{55}$$

$$V_{nm} \;=\; -\frac{4}{\pi}\beta^2\int_0^\pi \mathrm{d}\theta\,\sin n\theta\int_0^\pi \mathrm{d}\theta'\,\sin\theta'\sin m\theta'\,\mathrm{P}\frac{1}{(\cos\theta-\cos\theta')^2}\ . \tag{56}$$

Both of these integrals can be evaluated, with the result

$$(H_0)_{nm} \;=\; 4\,\min(n,m)\left[(-1)^{m+n}m_1^2+m_2^2\right], \tag{57}$$

$$V_{nm} \;=\; V_{n-1,m-1}\left(\frac{m}{m-1}\right)+\frac{8m}{n+m-1}\left[\frac{1+(-1)^{n+m}}{2}\right], \tag{58}$$

where $V_{n0}=V_{0m}=0$ for $m,n\geq 0$. This recursive form for V_{nm} is most convenient for numerical calculations; however, one may also write the closed-form solution,

$$V_{nm} = 4m\left[\frac{1+(-1)^{n+m}}{2}\right]\left[\psi\left(\frac{1-n-m}{2}\right)-\psi\left(\frac{1-|n-m|}{2}\right)\right]. \tag{59}$$

Note that the "potential" V in Eq. (59) is real but not symmetric, owing to the extra $\sin\theta'$ in Eq. (56); therefore, the "Hamiltonian" H_0+V is not Hermitian, and the eigenvectors $a^{(p)}$ are not orthogonal. This is a direct result of converting the exact

wavefunctions, which are eigenfunctions of a Hermitian Hamiltonian when written in terms of the variable x (and therefore orthogonal in x), into orthogonal functions of the variable θ. This transformation is nonunitary because the number of modes used is not infinite; therefore, the overlap of different eigenvector solutions should be small when a large number of modes are used. Indeed, this turns out to be empirically true; nevertheless, we take the further step of orthogonalizing the numerical eigenvector solutions recursively by means of the standard Gram-Schmidt procedure, i.e.,

$$\left|\varphi^{(p)}_{\rm orth}\right\rangle = \frac{\left|\varphi^{(p)}\right\rangle - \sum_{j=0}^{p-1}\left|\varphi^{(j)}_{\rm orth}\right\rangle\left\langle\varphi^{(j)}_{\rm orth}\right|\,\varphi^{(p)}\right\rangle}{\sqrt{\left\langle\varphi^{(p)}\right|\,\varphi^{(p)}\right\rangle - \sum_{j=0}^{p-1}\left\langle\varphi^{(j)}_{\rm orth}\right|\,\varphi^{(p)}\right\rangle}}. \tag{60}$$

For $N = 500$ modes, this typically changes expectation values by one part in 10^5.

The expressions for these overlaps and other matrix elements in terms of the mode coefficients a_n are presented in Appendix B.

B Matrix Elements

A number of useful overlaps and other integrals are straightforward to evaluate in terms of the mode coefficients, using the expressions (52). Solving them amounts to evaluating a number of trigonometric integrals. Such expressions are especially convenient since they permit a number of integrations that introduce no numerical uncertainties (except due to machine precision) beyond those of solving the original Multhopp-BSW eigenvector equation (54).

In particular, denote the pth eigenstate wavefunction presented in Eq. (52) by $\varphi^{(a)}_p$ and that for some other set of masses in the qth eigenstate by $\varphi^{(b)}_q$; the latter wavefunction then has an expansion like (52) with mode coefficients $b^{(q)}_n$. Truncating after N modes, one then finds

$$\begin{aligned}\left\langle\varphi^{(a)}_p\right|\,\varphi^{(b)}_q\right\rangle &= \int_0^1 {\rm d}x\,\varphi^{(a)}_p(x)\varphi^{(b)}_q(x) \\ &= -2\sum_{m=1}^{N} m a^{(p)}_m \sum_{n=1}^{N} n b^{(q)}_n \left[\frac{1+(-1)^{m+n}}{2}\right]\frac{1}{[1-(m-n)^2]\,[1-(m+n)^2]}.\end{aligned} \tag{61}$$

Indeed, the normalization integral $\int_0^1 {\rm d}x\,\varphi(x)^2 = 1$ is just the case $a = b$ and $p = q$, in agreement with Eq. (A9) of Ref. [6].

Other useful expectation values include

$$\begin{aligned}\left\langle x-\frac{1}{2}\right\rangle_p &= \int_0^1 {\rm d}x\,\left(x-\frac{1}{2}\right)\left[\varphi^{(a)}_p(x)\right]^2 \\ &= -\sum_{m=1}^{N} m a^{(p)}_m \sum_{n=1}^{N} n a^{(p)}_n \left[\frac{1-(-1)^{m+n}}{2}\right]\frac{1}{[4-(m-n)^2]\,[4-(m+n)^2]},\end{aligned} \tag{62}$$

$$\left\langle \left(x-\frac{1}{2}\right)^2 \right\rangle_p = \int_0^1 \mathrm{d}x \, \left(x-\frac{1}{2}\right)^2 \left[\varphi_p^{(a)}(x)\right]^2$$
$$= -\frac{1}{2}\sum_{m=1}^{N} m a_m^{(p)} \sum_{n=1}^{N} n a_n^{(p)} \left[\frac{1+(-1)^{m+n}}{2}\right] \left[21-6(m^2+n^2)+(m^2-n^2)^2\right]$$
$$\times \left[\left(1-(m-n)^2\right)\left(1-(m+n)^2\right)\left(9-(m-n)^2\right)\left(9-(m+n)^2\right)\right]^{-1}. \qquad (63)$$

Note that the spread of the wavefunction may be computed about any convenient point in x, viz.,

$$\left\langle (ax+b)^2 \right\rangle - \left\langle (ax+b) \right\rangle^2 = a^2 \left(\left\langle x^2 \right\rangle - \left\langle x \right\rangle^2 \right), \qquad (64)$$

so that the additive constants of $-1/2$ above are irrelevant. Also,

$$\left\langle \frac{1}{x} \right\rangle_p = \int_0^1 \mathrm{d}x \, \frac{1}{x} \left[\varphi_p^{(a)}(x)\right]^2 = \sum_{m=1}^{N} a_m^{(p)} \sum_{n=1}^{N} a_n^{(p)} \, I_{mn}, \qquad (65)$$

where

$$I_{mn} = 2 \sum_{j=|m-n|/2}^{(m+n)/2-1} \frac{1}{2j+1}$$
$$= \psi\left(\frac{m+n+1}{2}\right) - \psi\left(\frac{|m-n|+1}{2}\right), \quad m-n \text{ even};$$
$$I_{mn} = \frac{1}{|m-n|} - \frac{1}{m+n} - 2 \sum_{j=(|m-n|-1)/2}^{(m+n-1)/2-1} \frac{1}{2j+1}$$
$$= \frac{1}{|m-n|} - \frac{1}{m+n} + \psi\left(\frac{|m-n|}{2}\right) - \psi\left(\frac{m+n}{2}\right), \quad m-n \text{ odd}. \qquad (66)$$

One also finds

$$\left\langle \frac{1}{1-x} \right\rangle_p = \int_0^1 \mathrm{d}x \, \frac{1}{1-x} \left[\varphi_p^{(a)}(x)\right]^2 = \sum_{m=1}^{N} a_m^{(p)} \sum_{n=1}^{N} a_n^{(p)} \, J_{mn} \, , \qquad (67)$$

where, using the notation of Eq. (66), one finds $J_{mn} = +I_{mn}$ for $m-n$ even, and $J_{mn} = -I_{mn}$ for $m-n$ odd.

Finally, the decay constant of the pth excitation [cf. Eqs. (10)–(11)] is given by

$$f_p^{(a)} = \sqrt{\frac{N_c}{\pi}} \int_0^1 \mathrm{d}x \, \varphi_p^{(a)}(x) = \sqrt{\frac{N_c}{\pi}} \, c_p = \sqrt{\frac{N_c}{\pi}} \times \frac{\pi}{4} \, a_1^{(p)} \, . \qquad (68)$$

C Additional Relations Used in the Analysis

The numerical calculation of large-m_Q matrix elements with acceptable accuracy relies on achieving a balance between competing effects.

On one hand, Multhopp solutions to the 't Hooft equation with $m_Q \gg \beta$ tend to suffer degraded numerical accuracy since they are highly concentrated into the small kinematic region $1-x \ll 1$. As discussed in Sec. 2, the endpoint regions $x \approx 0$ and 1 are where the Multhopp solutions—or more precisely, their derivatives—tend to break down. This effect is compounded when $m \ll \beta$, since lighter quark masses force sharper endpoint behavior in the wavefunction. Although the BSW solution ameliorates this behavior, as m_Q is increased one eventually faces the problem of attempting to represent a function with only a very small region of support in x by a finite number of modes with support over the full range $x \in [0,1]$. In practice, we gauge the errors committed through such "lattice spacing" effects by computing a given quantity with $N=500$ and noting the amount by which its value shifts if one uses instead $N=100$, and as expected, such errors become substantial (as much as a few percent) by the time one reaches $m_Q > 25\beta$ or $m < 0.4\beta$.

On the other hand, although numerical solutions with m_Q, $m \simeq O(\beta)$ have the highest numerical accuracy, they also have substantial $O(1/m_Q)$, $O(1/m_Q^2)$, etc. corrections that are difficult to disentangle.

We adopt an intermediate strategy of employing certain exact relations that hold for the 't Hooft solutions. To determine the relevant static expectation values, we solve the finite-m_Q heavy hadron mass expansion for $\overline{\Lambda}$ [Eq. (6)]:

$$M_{H_Q} - m_Q \;=\; \overline{\Lambda} + \frac{\mu_\pi^2 - \beta^2}{2m_Q} + \frac{\rho_D^3 - \rho_{\pi\pi}^3}{4m_Q^2} \;+\; O\!\left(\frac{\beta^4}{m_Q^3}\right) . \tag{69}$$

Neglecting the order term and using the relations [Eq. (9)]

$$\mu_\pi^2 = \frac{\overline{\Lambda}^2 - m^2 + \beta^2}{3} , \qquad \rho_D^3 = \frac{\beta^2 F^2}{4} , \qquad \rho_{\pi\pi}^3 = \frac{1}{36}\left[8\overline{\Lambda}(\overline{\Lambda}^2 - m^2 + \beta^2) + 3\beta^2 F^2\right] , \tag{70}$$

we thus arrive at an equation cubic in $\overline{\Lambda}$ that depends on F^2. We solve it at $m_Q = 15\beta$.

The asymptotic value of the scaled decay constant $F^{(n)} = \sqrt{m_Q}\, c_n$ must also be evaluated at a finite value of m_Q, thus including $1/m_Q$-suppressed pieces. We account for them explicitly using the expansion [11] [the first of Eqs. (14)]

$$\sqrt{m_Q}\, c_n = \left(1 - \frac{2[2\overline{\Lambda}^{(n)} - m(-1)^n]}{3m_Q}\right) F^{(n)} + O\left(\frac{\beta^{5/2}}{m_Q^2}\right) . \tag{71}$$

We likewise solve this equation for $F^{(n)}$ at $m_Q = 15\beta$.

Turning to the analysis of the SV sum rules Eqs. (22)–(25) in Sec. 4, we note that their rapid saturation demands an exceptionally high precision in evaluating both the oscillation strengths τ in the r.h.s. and the expectation values in the l.h.s. Reaching such an accuracy through direct computation seems impossible. Therefore, we use a number of identities to get meaningful results. First, we employ the expression for τ_{nk} in terms of ϵ_n, ϵ_k, and the corresponding decay constants:

$$\tau_{nk} = -\frac{\beta^2}{2(\epsilon_n - \epsilon_k)^3}\, F^{(n)} F^{(k)} \left(\frac{1-(-1)^{n-k}}{2}\right) . \tag{72}$$

Then we make use of the fact that the discussed sum rules, being completeness sums, are exact when summation includes all excitations (see Ref. [11]). Therefore, one has

$$\frac{1}{\rho_k^2-\frac{1}{4}}\left[\rho_k^2-\frac{1}{4}-\sum_{\ell=1}^{n}\tau_{\ell k}^2\right] = \frac{1}{\rho_k^2-\frac{1}{4}}\sum_{\ell=n+1}^{\infty}\tau_{\ell k}^2\,, \tag{73}$$

$$\frac{2}{\overline{\Lambda}_k}\left[\frac{1}{2}\overline{\Lambda}_k-\sum_{\ell=1}^{n}(\epsilon_\ell-\epsilon_k)\,\tau_{\ell k}^2\right] = \frac{2}{\overline{\Lambda}_k}\sum_{\ell=n+1}^{\infty}(\epsilon_\ell-\epsilon_k)\,\tau_{\ell k}^2\,, \tag{74}$$

$$\frac{1}{(\mu_\pi^2)_k}\left[\left(\mu_\pi^2\right)_k-\sum_{\ell=1}^{n}(\epsilon_\ell-\epsilon_k)^2\,\tau_{\ell k}^2\right] = \frac{1}{(\mu_\pi^2)_k}\sum_{\ell=n+1}^{\infty}(\epsilon_\ell-\epsilon_k)^2\,\tau_{\ell k}^2\,, \tag{75}$$

$$\frac{1}{(\rho_D^3)_k}\left[\left(\rho_D^3\right)_k-\sum_{\ell=1}^{n}(\epsilon_\ell-\epsilon_k)^3\,\tau_{\ell k}^2\right] = \frac{1}{(\rho_D^3)_k}\sum_{\ell=n+1}^{\infty}(\epsilon_\ell-\epsilon_k)^3\,\tau_{\ell k}^2\,. \tag{76}$$

The sums on the r.h.s. can be accurately evaluated since the higher contributions fall off in magnitude very quickly. In practice, we truncate the sum at $\ell=20$.

A similar approach was used to evaluate the duality-violating difference $\Gamma_B-\Gamma_{\rm OPE}$ as a function of m_Q. We use the exact relation [5] [Eqs. (34), (35), (38)]

$$\Gamma_B=\frac{G^2}{4\pi}\cdot\frac{m_b^2-m_c^2}{M_B}\int_0^1\frac{{\rm d}x}{x}\,\varphi_B^2(x)\,-\,\frac{G^2}{4\pi}\sum_{M_n>M_B}\frac{M_B^2-M_n^2}{M_B}\left|\int_0^1{\rm d}x\,\varphi_n(x)\varphi_B(x)\right|^2, \tag{77}$$

and therefore,

$$\frac{\Gamma_B-\Gamma_{\rm OPE}}{\Gamma_{\rm OPE}}=\left(\int_0^1\frac{{\rm d}x}{x}\,\varphi_B^2(x)\right)^{-1}\sum_n\,\frac{M_n^2-M_B^2}{m_b^2-m_c^2}\left|\int_0^1{\rm d}x\,\varphi_n(x)\varphi_B(x)\right|^2\theta(M_n-M_B)\,. \tag{78}$$

The summation runs over all final excited states kinematically *forbidden* in the decay. Once again, the sum converges rapidly and is dominated by the lowest couple of states.

References

[1] G. 't Hooft, Nucl. Phys. **B75**, 461 (1974).

[2] E.C. Poggio, H.R. Quinn and S. Weinberg, Phys. Rev. D **13**, 1958 (1976).

[3] M. Shifman, "Theory of Preasymptotic Effects in Weak Inclusive Decays," in Proc. Workshop on *Continuous Advances in QCD*, ed. A. Smilga (World Scientific, Singapore, 1994), p. 249 [hep-ph/9405246].

[4] B. Chibisov, R. Dikeman, M. Shifman and N.G. Uraltsev, Int. Journ. Mod. Phys. **A12**, 2075 (1997).

[5] I. Bigi, M. Shifman, N. Uraltsev and A. Vainshtein, Phys. Rev. D **59**, 054011 (1999).

[6] B. Grinstein and R.F. Lebed, Phys. Rev. D **57**, 1366 (1998).

[7] B. Grinstein and R.F. Lebed, Phys. Rev. D **59**, 054022 (1999).

[8] I. Bigi and N. Uraltsev, Phys. Rev. D **60**, 114034 (1999).

[9] I. Bigi and N. Uraltsev, Phys. Lett. B **457**, 163 (1999).

[10] M. Burkardt, Phys. Rev. D **46**, R1924 and R2751 (1992).

[11] M. Burkardt and N. Uraltsev, Univ. Notre Dame Report No. UND-HEP-00-BIG 03 [hep-ph/0005278].

[12] N. Isgur, Phys. Lett. B **448**, 111 (1999); Phys. Rev. D **60**, 074030 (1999).

[13] See, for example, K. Karamcheti, *Principles of Ideal-Fluid Aerodynamics*, John Wiley & Sons, New York, 1966.

[14] A.J. Hanson, R.D. Peccei, and M.K. Prasad, Nucl. Phys. **B121**, 477 (1977).

[15] R.C. Brower, W.L. Spence, and J.H. Weis, Phys. Rev. D **19**, 3024 (1979).

[16] I.I. Bigi, M. Shifman, N.G. Uraltsev and A. Vainshtein, Int. J. Mod. Phys. **A9**, 2467 (1994).

[17] D. Dikeman, M. Shifman and N.G. Uraltsev, Int. J. Mod. Phys. **A11**, 571 (1996).

[18] I. Bigi, M. Shifman, N. Uraltsev and A. Vainshtein, Phys. Rev. D **52**, 196 (1995).

[19] M. Burkardt and E. Swanson, Phys. Rev. **D46** (1992) 5083.

[20] K. Melnikov and A. Yelkhovsky, Phys. Rev. D **59**, 114009 (1999); A.H. Hoang, Phys. Rev. D **61**, 034005 (2000).

[21] M. Voloshin, Surv. High En. Phys. **8**, 27 (1995).

[22] I. Bigi, M. Shifman and N.G. Uraltsev, Ann. Rev. Nucl. Part. Sci. **47**, 591 (1997) [hep-ph/9703290].

[23] N. Uraltsev, preprint UND-HEP-98-BIG1, in *Heavy Flavour Physics: A Probe of Nature's Grand Design*, Proceedings of the International School of Physics "Enrico Fermi," Course CXXXVII, Varenna, July 7-18, 1997, eds. I. Bigi and L. Moroni (IOS Press, Amsterdam, 1998) p. 329 [hep-ph/9804275].

[24] M. Voloshin and M. Shifman, Yad. Fiz. **47**, 801 (1988) [Sov. J. Nucl. Phys. **47**, 511 (1988)].

[25] R.D. Dikeman, N.G. Uraltsev, Nucl. Phys. **B509**, 378 (1998).

[26] I. Bigi, R.D. Dikeman, N. Uraltsev, Eur. Phys. J. **C4**, 453 (1998).

[27] "The BABAR Physics Book," eds. P.F. Harrison and H.R. Quinn, Rep. No. SLAC-R-504, Stanford Linear Accelerator, Stanford, CA, 1998.

[28] N. Uraltsev, Int. Journ. Mod. Phys. **A14**, 4641 (1999).

m_Q	$M_{H_Q} - m_Q$	$\sqrt{m_Q}\lvert c_n\rvert$	$m_Q\langle 1-x\rangle$	$m_Q^2\,(\langle x^2\rangle - \langle x\rangle^2)$	$\frac{m_Q}{M_{H_Q}}\langle\frac{1}{x}\rangle - 1$
Ground state ($n=0$)					
0.56	1.21918	0.7300	0.280	0.017	8.34×10^{-2}
1.0	1.24633	0.9534	0.432	0.048	4.59×10^{-2}
3.0	1.28764	1.4210	0.791	0.211	9.04×10^{-3}
5.0	1.29904	1.6061	0.944	0.333	3.58×10^{-3}
7.0	1.30423	1.7503	1.029	0.417	1.88×10^{-3}
10.0	1.30820	1.7901	1.102	0.500	9.33×10^{-4}
15.0	1.31131	1.8633	1.166	0.582	4.14×10^{-4}
25.0	1.31375	1.9271	1.222	0.661	1.46×10^{-4}
35.0	1.31475	1.9560	1.248	0.700	7.31×10^{-5}
50.0	1.31545	1.9783	1.268	0.732	3.53×10^{-5}
First excited state ($n=1$)					
0.56	2.82831	0.0000	0.280	0.032	-1.30×10^{-1}
1.0	2.77888	0.0922	0.476	0.091	-9.62×10^{-2}
3.0	2.66569	0.4429	1.094	0.457	-3.29×10^{-2}
5.0	2.61977	0.6427	1.437	0.775	-1.60×10^{-2}
7.0	2.59522	0.7648	1.649	1.014	-9.40×10^{-3}
10.0	2.57436	0.8775	1.848	1.267	-5.14×10^{-3}
15.0	2.55644	0.9812	2.033	1.529	-2.50×10^{-3}
25.0	2.54088	1.0765	2.205	1.797	-9.68×10^{-4}
35.0	2.53382	1.1213	2.287	1.933	-5.10×10^{-4}
50.0	2.52833	1.1566	2.351	2.046	-2.56×10^{-4}

Table 1: Matrix elements as functions of heavy quark mass m_Q and light quark mass $m = 0.56\beta$, computed numerically via the BSW-improved Multhopp technique. All masses are in units of β.

m_Q	$M_{H_Q} - m_Q$	$\sqrt{m_Q}\,c_0$	$m_Q\langle 1-x\rangle$	$m_Q^2\,(\langle x^2\rangle - \langle x\rangle^2)$	$\frac{m_Q}{M_{H_Q}}\langle\frac{1}{x}\rangle - 1$
0.26	0.81299	0.5067	0.130	0.005	3.61×10^{-1}
1.0	0.92634	0.9481	0.373	0.050	7.60×10^{-2}
3.0	0.99222	1.3788	0.658	0.202	1.40×10^{-2}
5.0	1.00958	1.5420	0.772	0.306	5.40×10^{-3}
7.0	1.01725	1.6277	0.833	0.375	2.80×10^{-3}
10.0	1.02288	1.6999	0.885	0.442	1.38×10^{-3}
15.0	1.02692	1.7612	0.930	0.509	6.51×10^{-4}
25.0	1.02946	1.8137	0.969	0.591	3.42×10^{-4}
35.0	1.03003	1.8369	0.987	0.665	2.96×10^{-4}
50.0	1.02992	1.8543	1.002	0.811	2.97×10^{-4}

Table 2: The same matrix elements as in Table 1 for the ground state and $m = 0.26\beta$.

m	M_{H_Q}	$\left\langle \frac{1}{1-x} \right\rangle$	$\frac{m}{M_{H_Q}} \left\langle \frac{1}{1-x} \right\rangle - 1$
		$m_Q = 7\beta$	
0.10	7.84710	73.0	-7.0×10^{-2}
0.26	8.01725	31.1	$+9.4 \times 10^{-3}$
0.40	8.15422	19.2	-5.6×10^{-2}
0.56	8.30423	13.8	-6.7×10^{-2}
1.00	8.71728	8.24	-5.5×10^{-2}
1.50	9.19304	5.87	-4.3×10^{-2}
		$m_Q = 10\beta$	
0.10	10.85436	98.6	-9.2×10^{-2}
0.26	11.02288	42.6	$+4.5 \times 10^{-3}$
0.40	11.15925	26.2	-6.2×10^{-2}
0.56	11.30820	18.7	-7.4×10^{-2}
1.00	11.71817	11.0	-6.1×10^{-2}
1.50	12.19091	7.73	-4.8×10^{-2}
		$m_Q = 20\beta$	
0.10	20.86224	182.	-1.3×10^{-1}
0.26	21.02864	81.0	$+2.0 \times 10^{-3}$
0.40	21.16490	49.4	-6.7×10^{-2}
0.56	21.31284	34.9	-8.3×10^{-2}
1.00	21.71902	20.2	-7.0×10^{-2}
1.50	22.18785	14.0	-5.6×10^{-2}

Table 3: Ground-state matrix elements as functions of m, used to probe the expectation value of the light-quark scalar density $\langle H_Q \,|\, \bar{q}q \,|\, H_Q \rangle \,/ 2M_{H_Q}$.

k	ϵ_k	τ_{k0}	$\rho^2 - 1/4$	$\bar{\Lambda}$	μ_π^2	ρ_D^3
0	1.318	—	—	—	—	—
1	2.516	7.25×10^{-1}	6.2×10^{-3}	1.5×10^{-2}	3.6×10^{-2}	8.8×10^{-2}
3	3.989	5.36×10^{-2}	7.8×10^{-4}	2.7×10^{-3}	9.4×10^{-3}	3.3×10^{-2}
5	5.060	1.73×10^{-2}	2.2×10^{-4}	9.3×10^{-4}	4.1×10^{-3}	1.8×10^{-2}
7	5.949	8.37×10^{-3}	8.7×10^{-5}	4.3×10^{-4}	2.2×10^{-3}	1.1×10^{-2}
9	6.724	4.92×10^{-3}	4.1×10^{-5}	2.3×10^{-4}	1.2×10^{-3}	6.7×10^{-3}
11	7.421	3.24×10^{-3}	2.1×10^{-5}	1.3×10^{-4}	7.4×10^{-4}	4.3×10^{-3}
13	8.060	2.29×10^{-3}	1.1×10^{-5}	7.0×10^{-5}	4.4×10^{-4}	2.7×10^{-3}
15	8.653	1.71×10^{-3}	5.4×10^{-6}	3.6×10^{-5}	2.4×10^{-4}	1.5×10^{-3}
17	9.209	1.32×10^{-3}	2.1×10^{-6}	1.5×10^{-5}	1.0×10^{-4}	6.6×10^{-4}
19	9.735	1.05×10^{-3}	—	—	—	—

Table 4: Meson mass eigenvalues $\epsilon_k \equiv M_{H_Q}^{(k)} - m_Q$ and oscillator strengths τ as functions of excitation number k, for $m = 0.56\beta$. The value for a given nonperturbative matrix element for each k indicates the fractional amount remaining after saturating the corresponding sum rules Eqs. (22)–(25) by states n with $n \leq k$.

n	M_n	$\langle n\|H_Q\rangle$	Γ_n/Γ_{H_Q}	$\sum_{m=0}^{n}\Gamma_m/\Gamma_{H_Q}$
0	11.3082	0.96426	9.45×10^{-1}	0.9448313
1	12.5744	0.25996	5.36×10^{-2}	0.9984744
2	13.4495	0.044347	1.23×10^{-3}	0.9997062
3	14.1780	0.023927	2.74×10^{-4}	0.9999801
4	14.8095	0.005462	1.03×10^{-5}	0.9999903
5	15.3810	0.006617	9.49×10^{-6}	0.9999998
6	15.9043	0.001391	1.87×10^{-7}	1.0000000

Table 5: Illustration of the speed of saturation in excitation number n of the total hadronic width Γ_{H_Q} by partial widths Γ_n from exclusive channels of mass M_n. In this example, $m_Q=15\beta$, $m_q=10\beta$, and $m=0.56\beta$, for which $M_{H_Q}=16.3113\beta$.

m_q	N	$\Gamma_{H_Q}/\Gamma_{\rm OPE}-1$	Γ_{H_Q}/Γ_Q-1
5.0	18	1.4×10^{-8}	4.1×10^{-4}
6.0	16	1.2×10^{-7}	4.1×10^{-4}
7.0	13	3.2×10^{-7}	4.1×10^{-4}
8.0	11	6.3×10^{-7}	4.1×10^{-4}
9.0	8	1.2×10^{-6}	4.2×10^{-4}
10.0	6	2.2×10^{-6}	4.2×10^{-4}
11.0	4	4.3×10^{-6}	4.2×10^{-4}
12.0	3	9.0×10^{-6}	4.2×10^{-4}
12.5	2	2.1×10^{-5}	4.4×10^{-4}
13.0	1	3.2×10^{-5}	4.5×10^{-4}
13.5	1	3.4×10^{-5}	4.5×10^{-4}
14.0	0	5.9×10^{-4}	1.0×10^{-3}
14.5	0	8.4×10^{-4}	1.3×10^{-3}

Table 6: Numbers relevant to local duality violation for $m_Q=15\beta$, $m=0.56\beta$, and m_q variable. N indicates the excitation number of the heaviest final-state meson kinematically allowed for the given initial meson mass M_{H_Q}: $M_N\le M_{H_Q}<M_{N+1}$. Γ_{H_Q} is the total hadronic width Eq. (37), while $\Gamma_{\rm OPE}$ and Γ_Q are given by Eqs. (38) and (39), respectively.

m_q	N	$\Gamma_{H_Q}/\Gamma_{\rm OPE}-1$	Γ_{H_Q}/Γ_Q-1
5.0	6	6.9×10^{-6}	9.4×10^{-4}
5.5	5	8.6×10^{-6}	9.4×10^{-4}
6.0	4	1.3×10^{-5}	9.5×10^{-4}
6.5	3	1.8×10^{-5}	9.5×10^{-4}
7.0	3	2.1×10^{-5}	9.5×10^{-4}
7.5	2	5.5×10^{-5}	9.9×10^{-4}
8.0	1	7.6×10^{-5}	1.0×10^{-3}
8.5	1	7.9×10^{-5}	1.0×10^{-3}
9.0	0	1.4×10^{-3}	2.4×10^{-3}
9.5	0	1.9×10^{-3}	2.8×10^{-3}

Table 7: Same as in Table 6, except $m_Q=10\beta$.

m_q	N	$\Gamma_{H_Q}/\Gamma_{\rm OPE}-1$	Γ_{H_Q}/Γ_Q-1
1.0	3	8.5×10^{-5}	3.7×10^{-3}
1.5	3	8.0×10^{-5}	3.7×10^{-3}
2.0	2	1.9×10^{-4}	3.8×10^{-3}
2.5	2	2.5×10^{-4}	3.8×10^{-3}
3.0	1	3.5×10^{-4}	3.9×10^{-3}
3.5	1	3.2×10^{-4}	3.9×10^{-3}
4.0	0	6.6×10^{-3}	1.0×10^{-2}
4.5	0	7.3×10^{-3}	1.1×10^{-2}

Table 8: Same as in Table 6, except $m_Q=5\beta$.

m_Q	N	$\Gamma_{H_Q}/\Gamma_{\rm OPE}-1$	Γ_{H_Q}/Γ_Q-1
1.0	0	1.3×10^{-1}	1.8×10^{-1}
2.0	0	2.4×10^{-2}	4.2×10^{-2}
3.0	1	1.5×10^{-3}	1.1×10^{-2}
4.0	2	2.7×10^{-4}	5.7×10^{-3}
5.0	4	6.0×10^{-5}	3.6×10^{-3}
6.0	5	2.7×10^{-5}	2.6×10^{-3}
7.0	7	1.1×10^{-5}	1.9×10^{-3}
8.0	8	5.7×10^{-6}	1.5×10^{-3}
9.0	10	2.8×10^{-6}	1.2×10^{-3}
10.0	13	1.3×10^{-6}	9.3×10^{-4}
11.0	15	4.5×10^{-7}	7.7×10^{-4}
12.0	18	4.8×10^{-8}	6.5×10^{-4}

Table 9: Same as in Table 6, except $m_q=m=0.56\beta$ fixed and m_Q variable.

m_Q	N	$\Gamma_{H_Q}/\Gamma_{\rm OPE}-1$	Γ_{H_Q}/Γ_Q-1
1.0	0	2.2×10^{-1}	3.1×10^{-1}
2.0	1	1.2×10^{-3}	2.9×10^{-2}
3.0	1	1.1×10^{-3}	1.5×10^{-2}
4.0	2	1.9×10^{-4}	8.4×10^{-3}
5.0	4	5.2×10^{-5}	5.5×10^{-3}
6.0	5	2.4×10^{-5}	3.8×10^{-3}
7.0	7	1.0×10^{-5}	2.8×10^{-3}
8.0	8	5.1×10^{-6}	2.2×10^{-3}
9.0	10	2.5×10^{-6}	1.7×10^{-3}
10.0	12	1.1×10^{-6}	1.4×10^{-3}
11.0	15	4.2×10^{-7}	1.1×10^{-3}
12.0	17	5.2×10^{-8}	9.7×10^{-4}

Table 10: Same as in Table 9, except $m_q=m=0.26\beta$.

n	M_{2n}	$\bar{R}(M_{2n}^2)\times10^4$	$R_0(M_{2n}^2)\times10^4$
0	1.7792	930.5	805.6
1	4.5349	15.18	15.30
2	6.2796	4.082	4.099
3	7.6574	1.838	1.844
4	8.8310	1.037	1.040
5	9.8703	0.6635	0.6651
6	10.813	0.4602	0.4614
7	11.681	0.3376	0.3385
8	12.490	0.2581	0.2588
9	13.250	0.2036	0.2042

Table 11: Saturation of the vacuum current correlator as depicted graphically in Fig. 16. The fiducial q^2 point in each interval $M_{2n-1}^2<q^2<M_{2n+1}^2$, in which $\bar{R}$ (averaged hadronic δ-functions) and R_0 (Born-term partonic expression) are compared, is chosen to be M_{2n}^2.

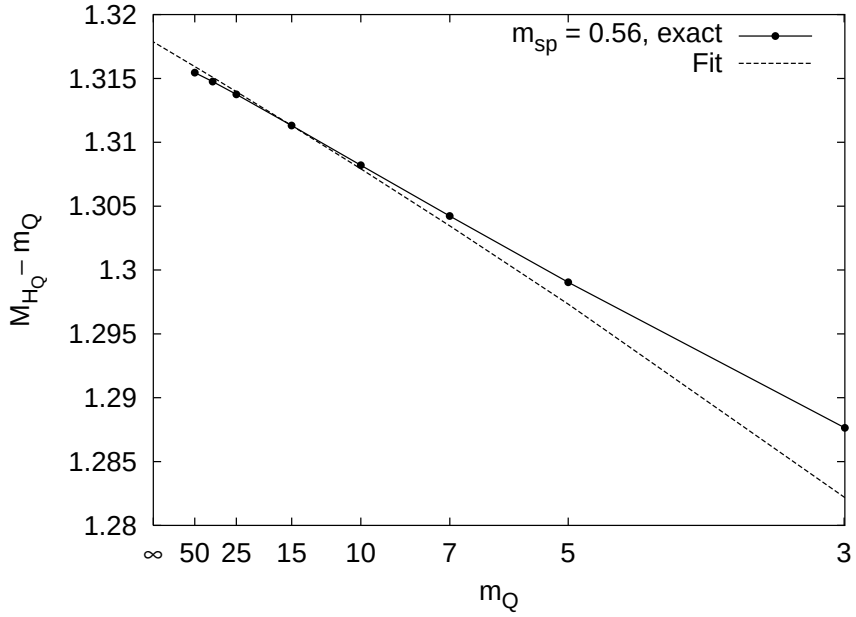

Figure 1: Values of the ground-state energy $M_{H_Q} - m_Q$ versus m_Q for $m = 0.56\beta$ determined through direct numerical calculation (solid line); fit of the mass expansion Eq. (6) to $O(1/m_Q^2)$, using the relations Eq. (9) and the approach described in Appendix C (dashed line).

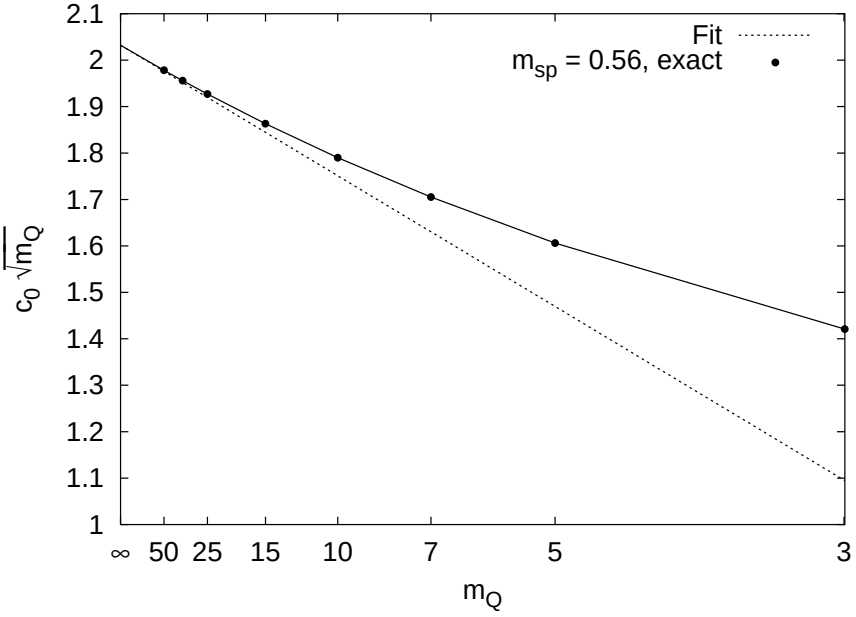

Figure 2: Values of the ground-state integral $c_0 \sqrt{m_Q}$ for $m = 0.56\beta$ (solid line). c_0 is related to the decay constant via Eq. (68). The dashed line represents an approximation using the first expansion in Eq. (14), good to $O(1/m_Q)$, and the asymptotic value F from a polynomial fit in $1/m_Q$ to the points on the solid line.

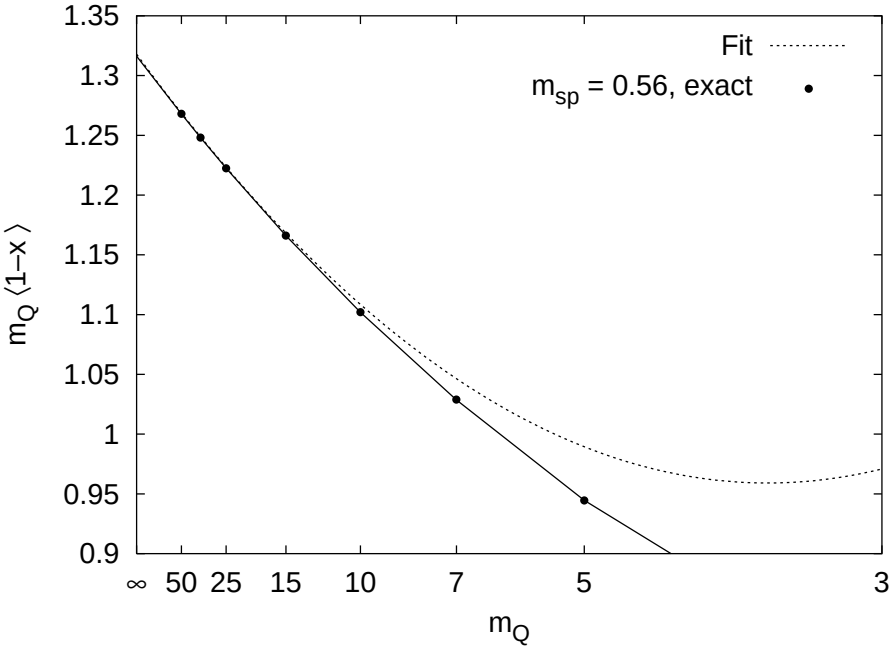

Figure 3: Values of the ground-state matrix element $m_Q\langle 1-x\rangle$ for $m=0.56\beta$ (solid line). The dashed line represents an approximation using the second expansion in Eq. (14), good to $O(1/m_Q^2)$.

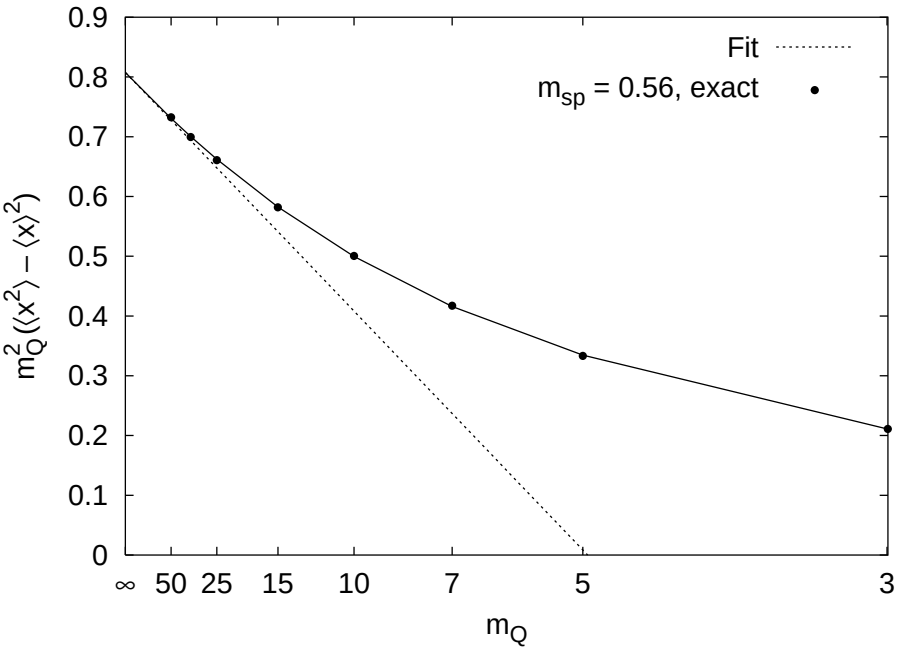

Figure 4: Values of the ground-state matrix element $m_Q^2(\langle x^2\rangle - \langle x\rangle^2)$ for $m=0.56\beta$ (solid line). The dashed line represents an approximation using the third expansion in Eq. (14), good to $O(1/m_Q)$.

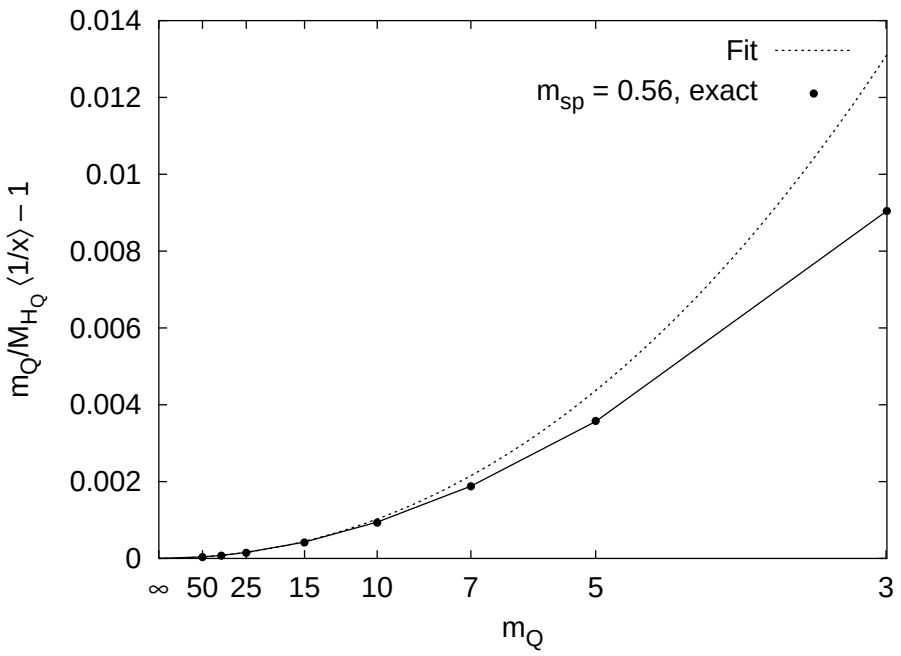

Figure 5: Values of the ground-state matrix element $(m_Q/M_{H_Q})\langle 1/x\rangle$–1 for $m=0.56\beta$ (solid line). The dashed line represents an approximation using the the final expansion in Eq. (14), good to $O(1/m_Q^3)$.

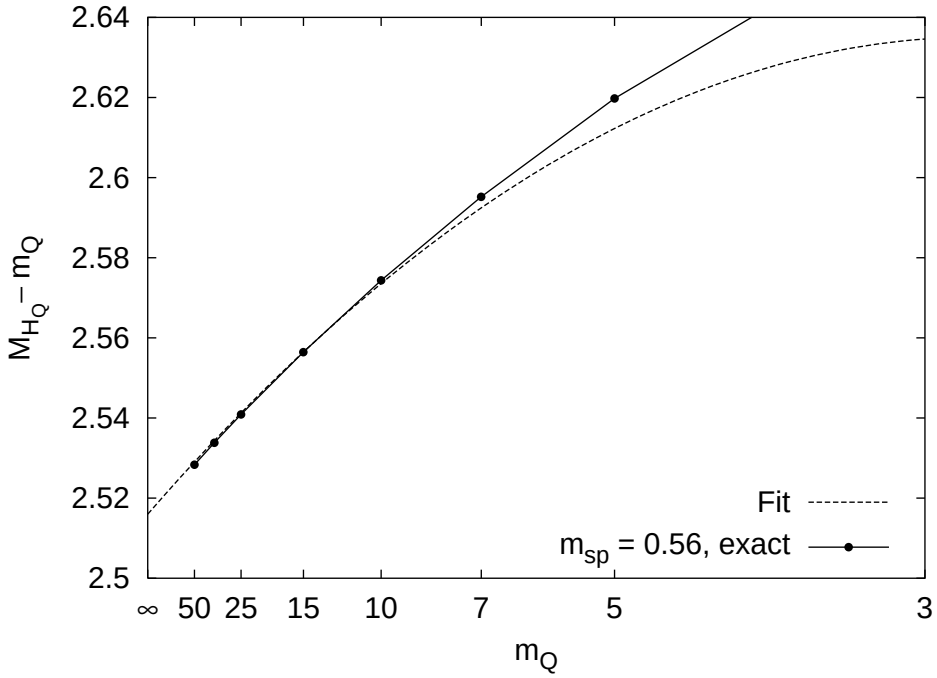

Figure 6: Same as in Fig. 1, except for the first excited state.

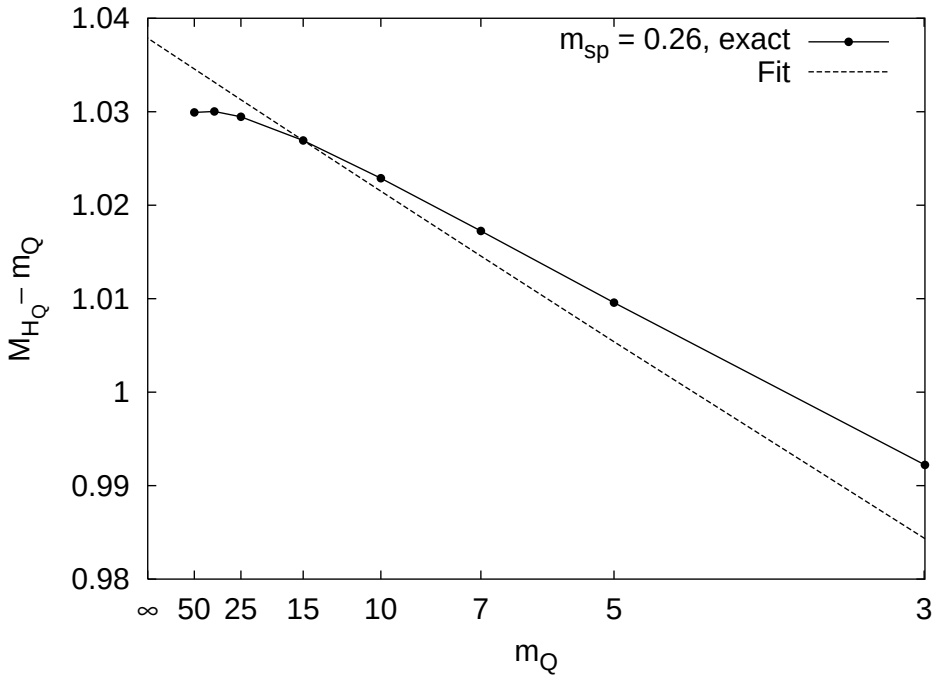

Figure 7: Same as in Fig. 1, except $m = 0.26\beta$.

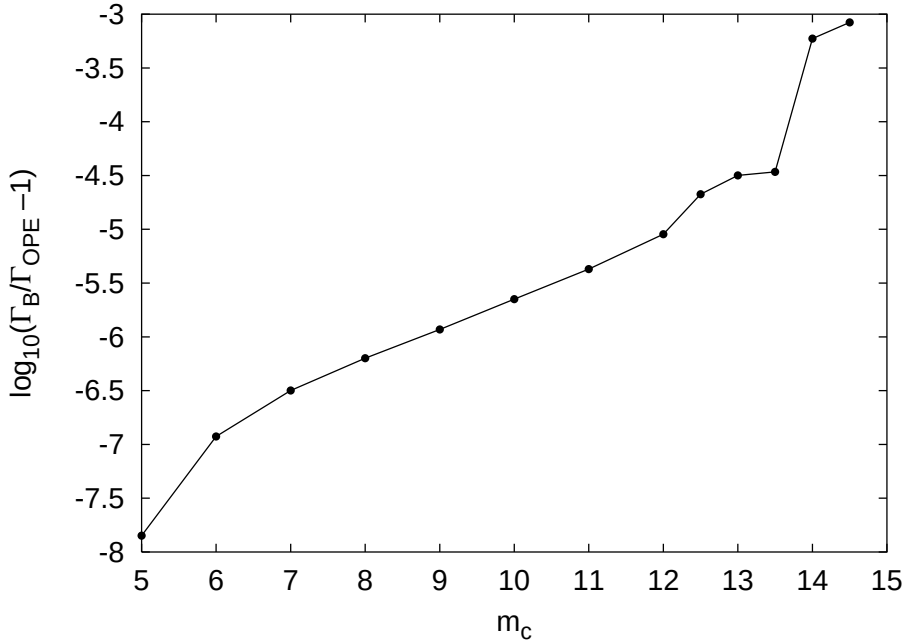

Figure 8: Duality deviation between exact hadronic width Γ_B and Γ determined from the OPE [Eq. (38) or (78)], good to $O(1/m_Q^4)$. Here $m_b = 15\beta$, $m = 0.56\beta$, and m_c variable.

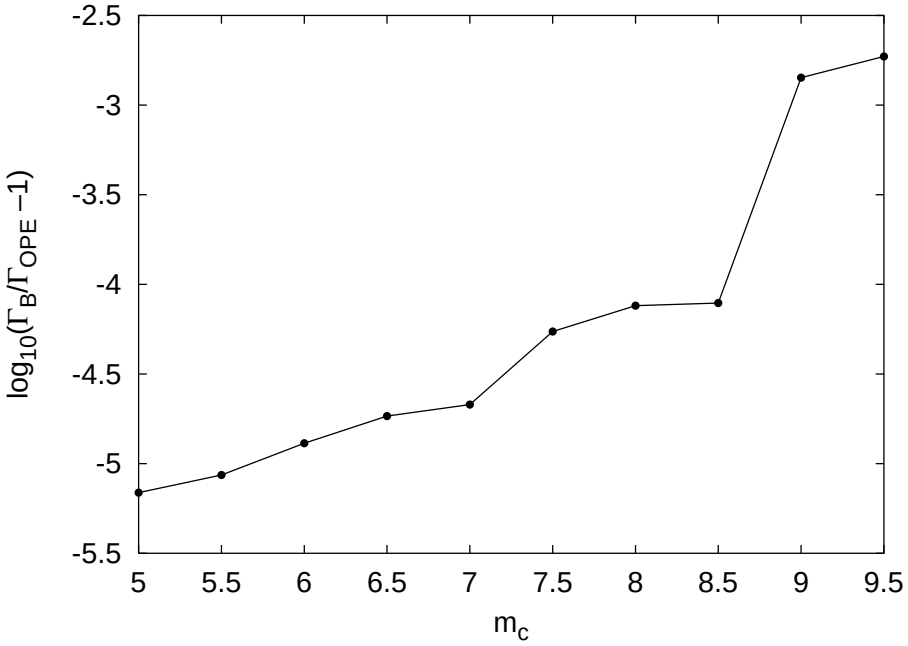

Figure 9: Same as Fig. 8, except $m_b = 10\beta$.

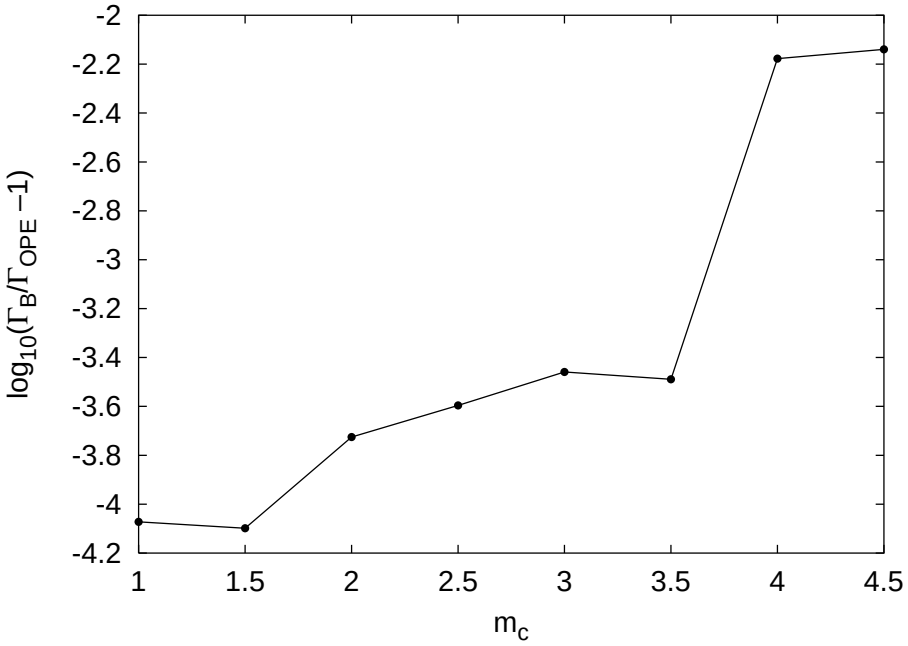

Figure 10: Same as Fig. 8, except $m_b = 5\beta$.

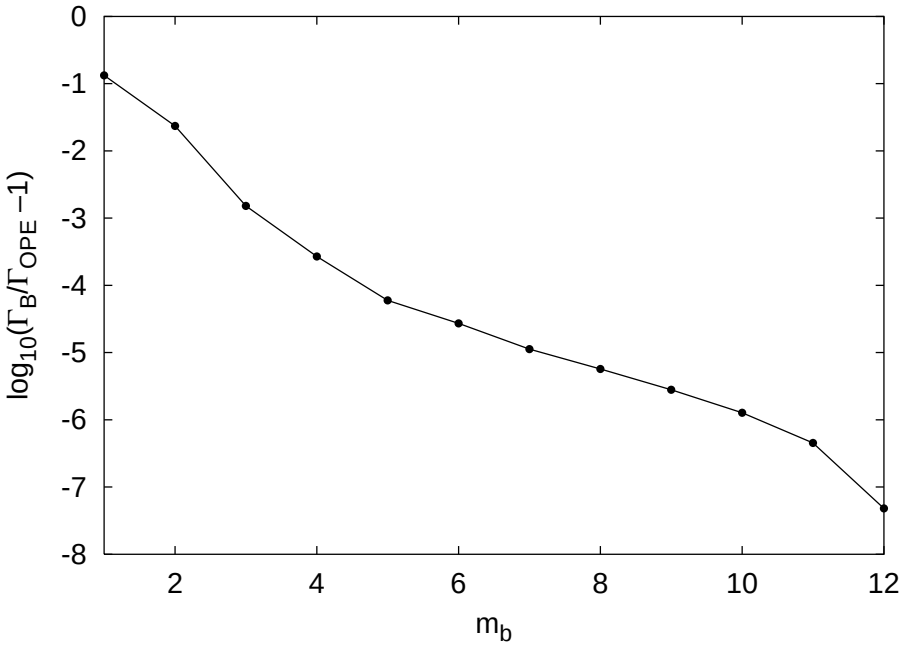

Figure 11: Same as Fig. 8, except $m_c = m = 0.56\beta$ and m_b variable.

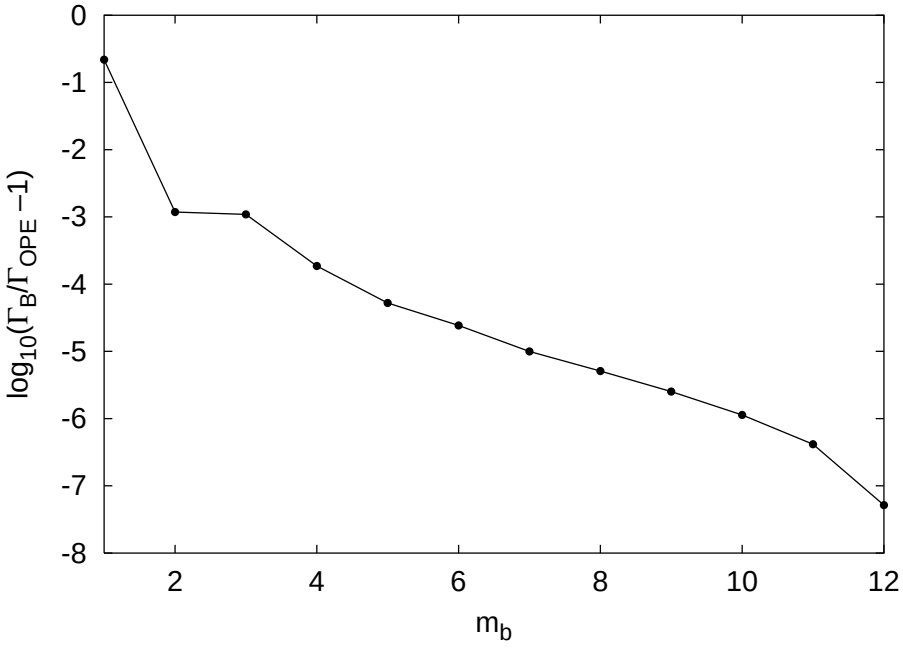

Figure 12: Same as Fig. 11, except $m_c = m = 0.26\beta$.

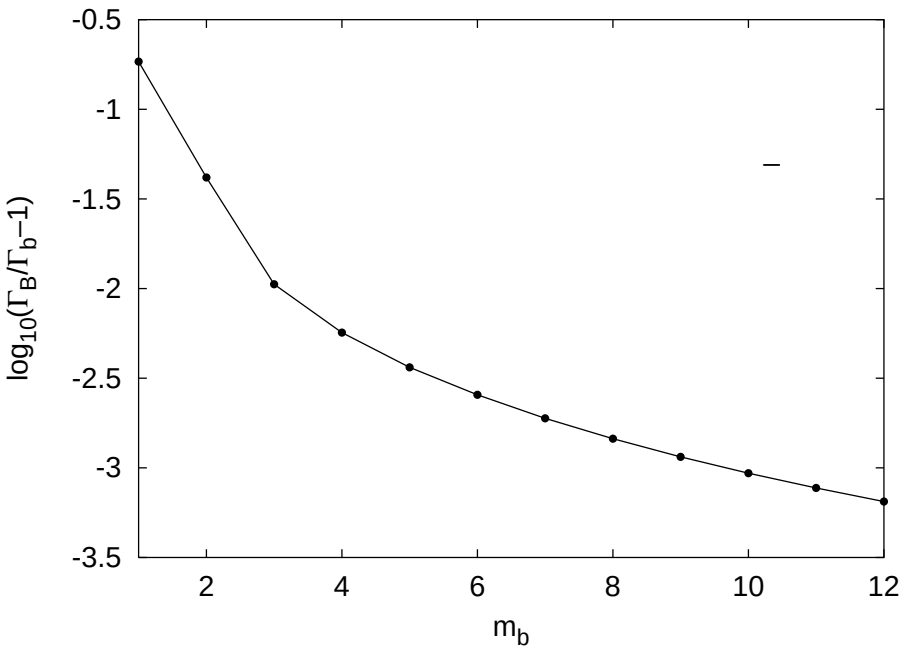

Figure 13: Same masses as in Fig. 11, using the Born-term partonic rate Γ_b instead of $\Gamma_{\rm OPE}$. Note that the deviation is much larger.

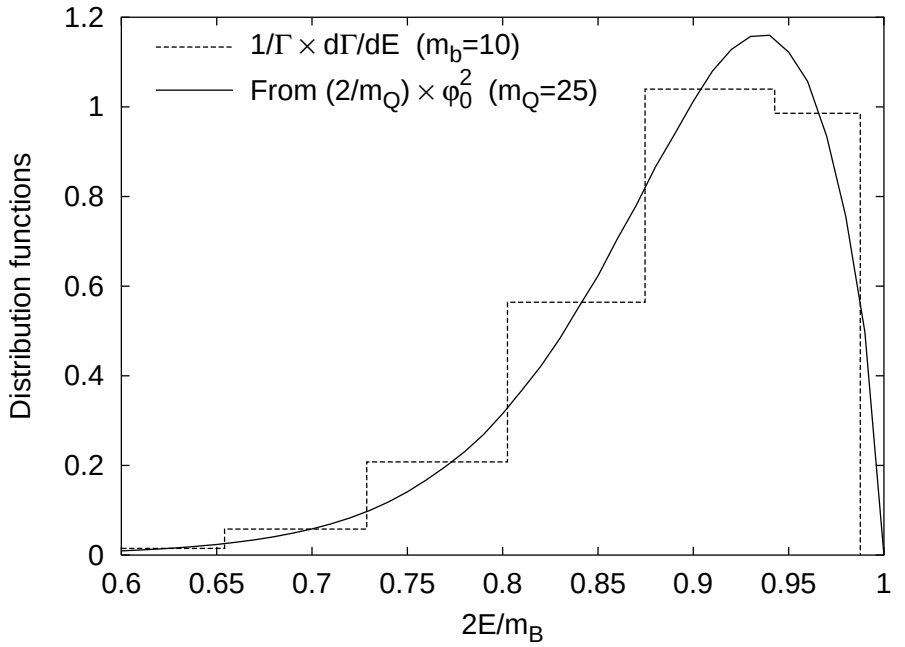

Figure 14: Exact differential width $\Gamma^{-1}\,{\rm d}\Gamma/{\rm d}E$, averaged as described in the text, compared to the continuous parton distribution computed via Eq. (43) with $m_Q = 25\beta$, at $m_b = 10\beta$ and $m = 0.56\beta$.

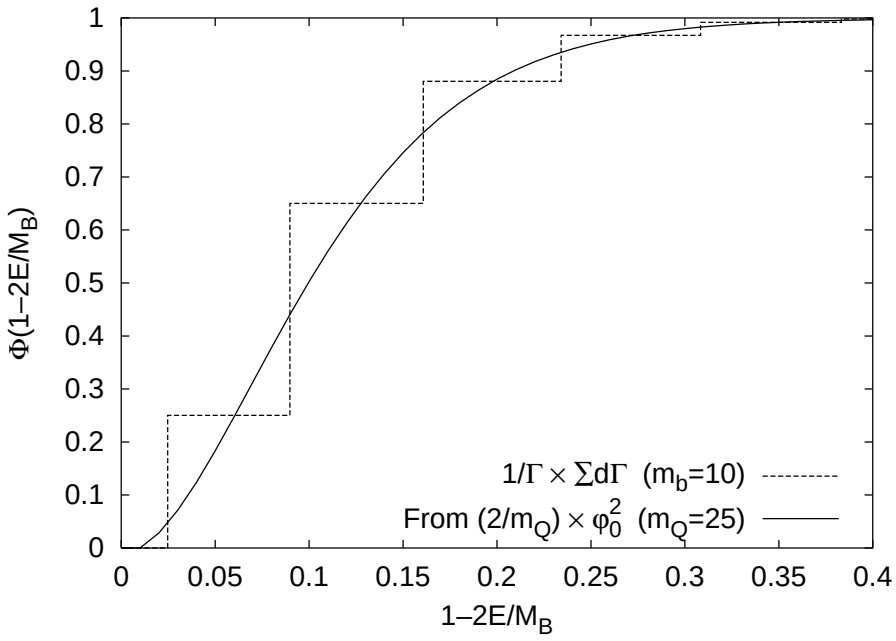

Figure 15: The partially-integrated (in E) differential distribution $\Phi(1{-}2E/M_B)$ and the corresponding smeared exact result $\Gamma^{-1}\sum \mathrm{d}\Gamma$ as defined in the text, for the same inputs as in Fig. 14.

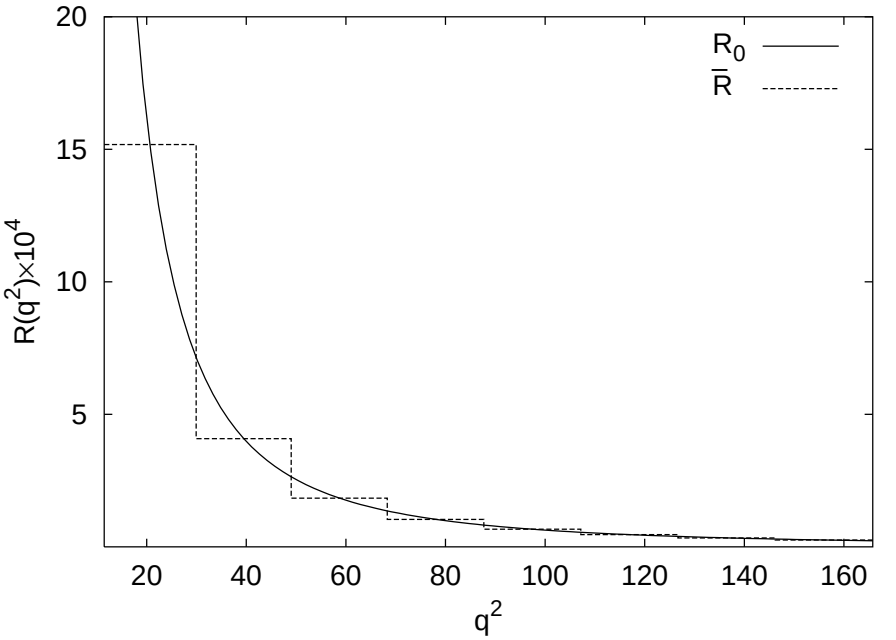

Figure 16: Saturation of the leading term in the OPE of the vacuum polarization function R_0 by exclusive channel δ-function contributions, smeared as described in the text ($\overline{R}$).